Characterization of the Degradation and Conversion of Bone Cement and Borate Bioactive Glass Composites

By
Kimberly Cole
B.S., University of Kansas, 2015

Submitted to the graduate degree program in Bioengineering and the Graduate Faculty of the University of Kansas in partial fulfillment of the requirements for the degree of Master of Science.

Chair: Dr. Terence McIff

Dr. Candan Tamerler

Dr. Paulette Spencer

Date Defended: December 8th, 2017

The thesis committee for Kimberly Cole certifies that this is the approved version of the following thesis:

Characterization of the Degradation and Conversion of Bone Cement and Borate Bioactive Glass Composites

Chair: Dr. Terence McIff

Date Approved: December 8th, 2017

Abstract

Periprosthetic infections are a devastating complication of orthopedic procedures, costing time and money as well as the quality of life of affected patients. 13-93B3 is a boron-based bioactive glass that degrades and converts into hydroxyapatite when immersed in a physiological fluid. Its ability to break down and dissolve quickly would be useful for drug delivery when combined with bone cement because this glass can create passages in the cement that would increase the elution of incorporated antibiotics. The conversion of this bioactive glass into calcium phosphate products could also attract surrounding bone growth, further integrating implants with tissue and removing space on the cement surfaces where biofilms can form. While bioactive glasses have previously been added to bone cement, the incorporation of 13-93B3 into commercial bone cement has not yet been reported in literature. The focus of this study was to characterize composites of these materials by measuring its degradation rate and the identity of its resulting precipitate while monitoring for adverse reductions of mechanical strength. Particles of 13-93B3 with diameters of 5 μm, 33 μm, and 100 μm were mixed into a PMMA-based commercial bone cement, DePuy SmartSet MV, to create composites with 20%, 30%, and 40% glass loadings. The composites were formed into pellets and paired with bone cement control groups. These samples were soaked in phosphate-buffered saline (PBS). The compressive strength, Young's modulus, water uptake, and weight loss of the pellets over time were recorded. The pH and boron concentrations of the solutions were measured at various soak durations. Results showed that smaller glass particles degraded faster in composites than larger particles, and that a higher amount of glass incorporation increased the amount of degradation that occurred. Composites with smaller glass diameters had higher compressive strengths than composites with larger glass particles, though the compressive strengths of all composites were found to be consistently above ASTM F451 and ISO 5833 standards. The conversion of 13-93B3 in the composites was studied using scanning electron microscopy (SEM), energy dispersive X-ray spectroscopy (EDS), Fourier transform infrared spectroscopy – attenuated total reflection (FTIR-ATR), and micro-Raman spectroscopy. The solid precipitate that accumulated on the surfaces was determined to be hydroxyapatite incorporated with magnesium ions from the dissolved glass. The presence of this magnesium in the hydroxyapatite layer could improve the adhesion of the bone cement to living bone. Results from these tests suggest that composites made of 13-93B3 and bone cement may have a promising future in helping to prevent periprosthetic infections and would benefit from further investigation.

Acknowledgements

This thesis was long in the making, and I couldn’t have done it as effectively as I did without the support and patience of Dr. Terence McIff and the rest of the orthopedic lab at KUMC during the process. I want to particularly thank Grahmm Funk and Damon Mar for helping me come out of my shell and giving me research pointers, and I would like to thank the orthopedic residents coming through the lab for their expertise. I am also thankful to the surgeons and nurses I observed at KUMC for showing me the human factors in their surgeries, as well as for the Department of Orthopedic Surgery at KUMC in general.

I have greatly appreciated my committee members supporting me and going over my thesis, and I am glad that they found my topic fascinating. I want to thank Dr. Mohamed Rahaman from Missouri University of Science and Technology for providing me with 13-93B3 glass particles at the sizes I was seeking, advising me on how to store the glass, and suggesting the middle glass size. I must also express my thanks to Dr. Gwen Macpherson for the use and operation of the ICP-OES equipment at the KU West Campus, Dr. James Murowchick for assisting with the SEM/EDS at UMKC, Barbara Fegley for the regular SEM usage at KUMC, and Dr. “Charles” Ye for showing me how to collect FTIR-ATR and Raman spectroscopy data at the BERC at KU.

I would like to thank the other students around me at KU, past and present, in bioengineering and otherwise, for accompanying me through graduate school and sharing their stories. I should also acknowledge the chemical engineering department at KU that molded me during my undergraduate years into the kind of person who would be interested in materials science and be capable enough to handle this thesis’s topic. I never really imagined at the time

that learning about spectroscopy and molecular vibrations would be relevant in my immediate future, and yet I worked in depth here to interpret infrared spectra.

Reading reference papers, compiling data, creating figures, and handling other work in graduate school was made a faster process by listening to Talking Heads, Kendrick Lamar, Bowie, and Brian Eno albums constantly on repeat. Various then-upcoming concerts motivated me to keep going and colored my life in these years, and I would like to thank my boyfriend Dennis Kruse for coming along with me on my trips to them. I am also thankful to him for listening to me repeatedly explain my thesis concept and giving me feedback and moral support.

I thank my family and friends in Lawrence and Kansas City for supporting and encouraging me wholeheartedly, even when they didn’t know what I was exactly doing, and particularly my sister Michelle Cole for putting up with my erratic sleeping patterns. Thanks again to Michelle for looking through my thesis and wondering how effective X-ray diffraction would have actually been for non-crystalline materials.

The work here was supported by the Marc A. and Elinor J. Asher Orthopedic Research Endowment.

Table of Contents

Chapter 3: Characterization of the Conversion of Bone Cement and Boron-Based Bioactive Glass Composites……………………………………………………………………..45

List of Figures

List of Tables

Chapter 1: Introduction

1.1. Burden of Prosthetic Joint Infections in the United States

The cartilage in a person's joint, such as in the hip or knee, can wear down over time. When this cartilage has degraded enough to cause pain and decreased mobility, the affected person can elect to undergo a joint arthroplasty to replace the damaged tissue with prosthetics. The main reason that this surgery is performed is to alleviate persistent pain from advanced arthritis that does not respond to less invasive measures.[1]

While a joint arthroplasty can solve the initial problem, complications can arise. Of prosthetic implantation surgeries, infection is the second leading complication after aseptic loosening.[2] In a study conducted in 2005 researching the reason that total knee replacement revisions occurred in 60,355 cases in the United States, the most common cause for a revision surgery was infection at 25.2%.[3] In all joint prosthetic surgeries, the incidence of infection occurs between 1.0 to 3.0% of the time.[4] Risk factors for developing infection include obesity, diabetes, rheumatoid arthritis, cancer, smoking, superficial infections at the surgical site, and using immunosuppressive medication.[5,6] These comorbidities leave patients more susceptible to developing infections around the implant.

Joint infections are distinguished from other complications using infection criteria, such as the development of a sinus tract next to the implant and bacterial growth in fluid cultures taken from the joint.[6-8] Once the complication is diagnosed as a periprosthetic infection, an orthopedic surgeon performs a joint revision by reopening the site and removing the implants and surrounding tissue to clear away the bacterial infection. In a one-stage revision for total knee arthroplasties, after cleaning the infected site, new implants are placed into position during the same surgery. In a two-stage revision, which is the more common type of joint revision performed in North America and is considered to be the more rigorous approach, after the infected implants are removed, a temporary spacer is placed into the patient where the implants had been.[5,8] The patient is given intravenous antibiotics for six weeks and then rest without antibiotics for at least two more weeks while being monitored for further signs of infection. Once the infection is declared cleared, another surgery is performed to take out the spacer and install new implants. Antibiotic-loaded bone cement is placed between the implant and the bone to help prevent a new infection.[5,8,9] In 2007, the two-stage revision was reported to be more effective at clearing bacteria from the knee (91%) than the one-stage revision (81.1%).[10] While a revision surgery may eliminate microbes, the quality of life for the patient can decrease. Twenty percent of patients in one study were unable to regain the functional use of their limb after a revision surgery.[11] In patients undergoing joint revisions, the amount of bone left at the joint is reduced after each revision due to some bone being removed along with the infected implant. Therefore, the number of possible revisions that can be performed is finite. The inability to control the infection forces other options to be considered, such as removing the implants without replacing them (resection arthroplasty), fusing the joint into a fixed position (arthrodesis), or, when severe bone and tissue loss has occurred, amputation.[5,8,12]

The average total cost of treating an infected joint in 2009 was $74,900 for knee patients and $93,600 for hip patients. In the same year, the cost of performing follow-up treatments to prosthetic hip and knee replacements was $566 million in the United States, and this number was expected to rise to $1.6 billion by 2020.[13] A study was conducted in 2005 to follow the trends in knee and hip revisions in the United States from 1990-2003, and this research predicted that in 2030, 572,000 hip arthroplasties and 3.48 million knee arthroplasties would be performed. Along with this, the study predicted that 96,700 hip revisions and 268,200 knee revisions would occur in the United States in 2030, which would be a 174% and 601% increase from values seen in 2005, respectively.[14] Because of this forecasted rise in total surgeries, reducing the demand for revision surgery in the growing pool of arthroplasty patients would substantially lower healthcare costs in the future.

1.2. Clinical Use of Bone Cement and Introduction to DePuy SmartSet Bone Cement

Bone cement is a hard, inorganic polymer-based material used by surgeons as a grout to fill gaps in bone and around metal implants placed into joints. Various medical device companies create their own formulations of bone cement.[15] Commercial bone cement is primarily made of poly(methyl methacrylate), known as PMMA, and contains other components in lesser amounts. These fillers are meant to improve the properties of the cement, such as by accelerating the polymerization of the PMMA and controlling its viscosity.[16] The use of acrylic (PMMA-based) bone cement to anchor joint implants to bone was started by Charnley in the late 1950s and continues today.[17]

One such commercial bone cement is DePuy SmartSet MV (DePuy, Warsaw, IN), the acrylic bone cement that will be studied in this thesis. SmartSet MV is packaged with a liquid and a solid component that forms a cement when mixed together. The liquid is composed of 98 wt.% methyl methacrylate, the monomer of PMMA, and 75 ppm hydroquinone, which acts as a stabilizer for storage by inhibiting polymerization. The remainder of the liquid is N,N-Dimethyl-p-toluidine, a curing activator.[18] The solid component is 67.05 wt.% methyl methacrylate monomer; 21.1 wt.% methyl methacrylate/styrene copolymer, which are beads of pre-polymerized material meant to increase fatigue strength; 1.85 wt.% benzoyl peroxide, a polymerization initiator; and 10 wt.% barium sulfate, a radiopacifier that increases the visibility of the bone cement in x-ray images.[19,20,21] Medical device companies aside from Depuy Synthes sell acrylic bone cements that contain similar ingredients in varying amounts.[15]

To initiate PMMA polymerization, N,N-Dimethyl-p-toluidine from the liquid component of SmartSet MV interacts with the benzoyl peroxide in the powder and cleaves this molecule into two benzoates, creating free radicals in the process (Figure 1-1).[16,22] Methyl methacrylate monomers then undergo free radical polymerization. Benzoyloxy radicals are the primary chain initiator, but the DMPT-related radical also contributes to initiation.[23] As the polymer forms and hardens, the material shifts from a viscoelastic material into one that is solid and primarily elastic.[16]

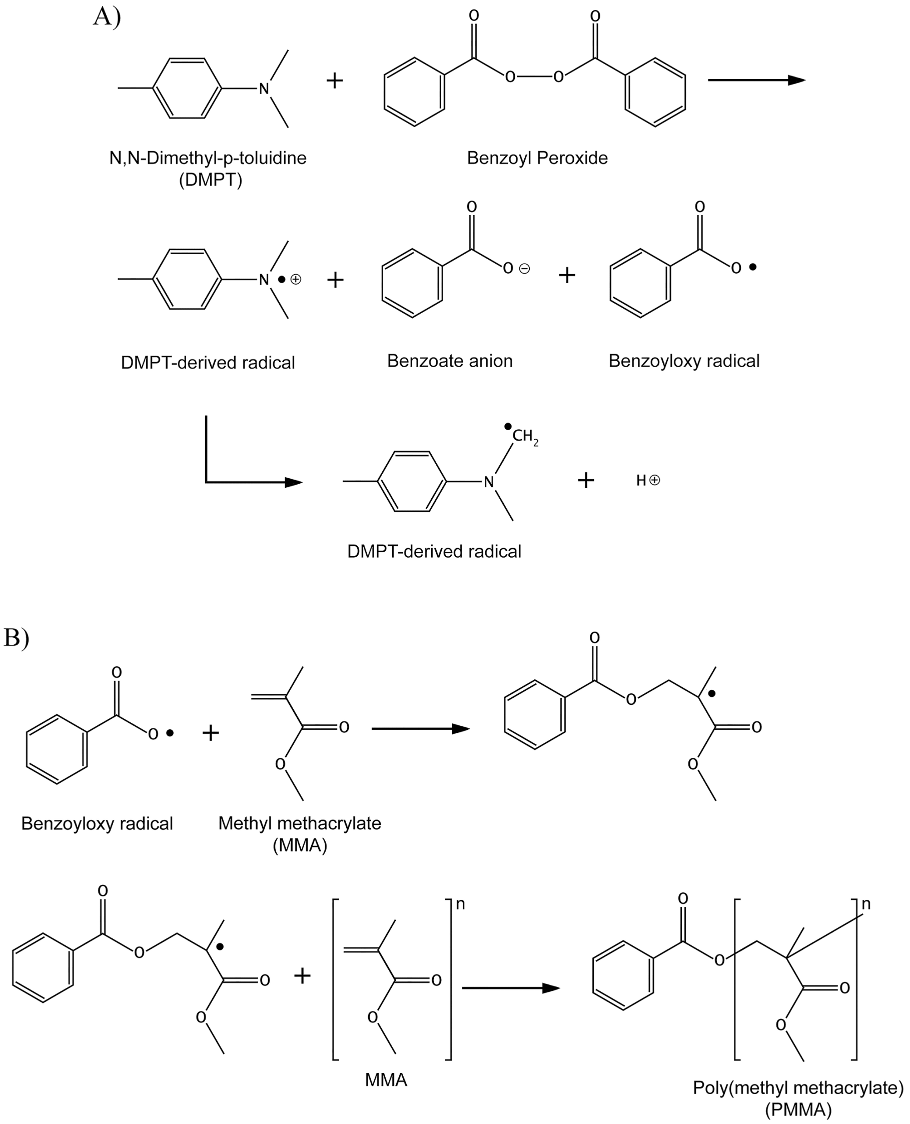

Figure 1-1: The cleaving of benzoyl peroxide by N,N-dimethyl-p-toluidine to form radicals (A) and the free radical polymerization reaction of methyl methacrylate monomer into poly(methyl methacrylate) (B).[16]

Antibiotics were first added to bone cement in 1969, and this combination has become the gold standard for antibiotic delivery when implant infection is a concern.[16,24] In recent years, packaged bone cement already loaded with gentamicin or tobramycin have been sold in the US.[25] Other antibiotics, such as vancomycin to target MRSA, are also regularly added into bone cement in the surgical room in the hopes that the antibiotic will leach out of the cement and prevent an infection from developing.[5] The FDA only approves antibiotic-loaded bone cement for use in the final stage of a second-stage revision after the infection has been cleared, but some doctors have used antibiotic bone cement for primary total joint replacements in an attempt to more thoroughly prevent infections.[26,27]

Despite its widespread use, antibiotic delivery using bone cement has limitations. Once the bone cement has been set in place and cured, an initial burst of antibiotic release occurs on the surface of the bone cement, and most of the remaining antibiotics typically become trapped in the cement.[28] The release of antibiotics from cement is mainly a surface phenomenon, and antibiotics leave the cement through cracks and pores that have been penetrated by fluid surrounding the cement.[29-31] After the initial release, only a small amount of antibiotics from within the cement is eluted, and this low concentration can allow for bacteria to develop a resistance against the antibiotic.[32]

Bone cement also provides a foreign surface inside the body where opportunistic bacteria, such as *Staphylococcus aureus* that entered the body during the surgery, can form biofilms. Biofilms are extracellular structures of polysaccharides and proteins that bacteria exude that allow them to adhere to surfaces, and the biofilm forms a protective barrier for the bacteria from the body's immune system and other external forces. Bacteria living within biofilms are more difficult to remove than free-floating bacteria through antibiotics.[33] Along with being housed in a protective slime, some bacteria living deep inside a biofilm can grow slowly and avoid antibiotic mechanisms that exploit cellular growth, and bacteria in a biofilm are able to work together using quorum sensing (chemical signaling) to coordinate gene expression against antibiotics.[34,35] The interface between acrylic bone cement and tissue tends to have either a gap or the presence of a fibrous tissue made in response to a foreign object in the body, which slows down the immune response in that area and can allow bacteria to quietly fester in biofilms until it is too late for the immune system to clear out the bacteria on its own.[36-38] Therefore, it is important to proactively eradicate bacteria before they are able to form protective biofilm hideouts and require more complex methods of treatment, such as joint revisions.

Antibiotic delivery through acrylic bone cement itself has had challenges in preventing biofilm formation. Dunne et al. discovered that adding large amounts of gentamicin to Palacos R bone cement (Heraeus-Kulzer, Hanua, Germany) reduced bacteria viability for several hours, but this ultimately did not prevent biofilm formation from *Staphylococcus aureus*, and that adding as much as 2 grams of gentamicin to the cement caused the compressive strength of the cement to fall below the ASTM F451 standard of 70 MPa.[39,40] Biofilms have also been found on gentamicin-loaded bone cement used clinically, meaning that they offer only a temporary avoidance of biofilms before their antibiotic elution rates are too low to suppress them.[25,41] Therefore, there is room for improvement to prevent biofilm formation on the surface of bone cement.

1.3. Introduction to Bioactive Glass

Bioactive glasses are resorbable materials that can degrade and convert into a hydroxyapatite-like material when in a physiological solution. Once inside the body, bioactive glasses attach to tissues and encourage growth from nearby bone due to their composition.[42,43] Bioactive glasses have been extensively researched as delivery carriers for antibiotics and nanoparticles.[44-49] The first bioactive glasses were composed of silicate, and their compositions have been experimented with to improve their qualities. The original bioactive glass formulation, Bioglass 45S5, was created by Dr. Larry Hench in 1969 at the University of Florida.[50] Bioglass

45S5 has been used in medical applications as a tissue scaffold.[51] Another silicon-based bioactive glass, 13-93, contains other oxides that allow for easier manufacturing by increasing the temperature range that the glass can be molded, and this glass is approved for *in vivo* use in Europe and in the USA.[52-54] The bioactive glass formulation S53P4 is particularly effective at eradicating a broad spectrum of bacteria, including *Staphylococcus aureus* and *Staphylococcus epidermidis*, which are common pathogens in periprosthetic infections.[5,55] Bioactive glasses all have antimicrobial properties to some extent, however. Their mechanism of action is thought to be the increase in pH and osmotic pressure caused by the dissolution of alkali metals such as Na, which is not favorable for bacterial growth and may affect bacteria membrane potential.[55] The optimal pH for most bacteria to form biofilms is 7, and deviations from this caused by bioactive glass can slow down biofilm formation.[56] A faster degradation rate may increase the antimicrobial properties of a glass by raising the pH and ionic concentrations in solution higher, but this relation has not been shown conclusively in literature and is likely dependent upon the glass composition.[57]

The degradation rate of a bioactive glass can be tailored by changing its composition. Increasing the ratio of boron to silicon causes the glass to degrade faster, which may be helpful for specialized applications.[58-60] 13-93B1 is a borosilicate bioactive glass manufactured in Mo-Sci, Corp. in Rolla, Missouri, that is derived from 13-93 by replacing approximately one-third of the SiO_2 in 13-93 with B_2O_3 (Table 1-1). The glass formulation that is the focus of this work is 13-93B3, which is borate-based and is the result of replacing all SiO_2 in 13-93 with B_2O_3. 13-93B3 degrades faster than 13-93B1, which degrades faster than 13-93.[52,61]

Glass	Na_2O	K_2O	MgO	CaO	SiO_2	B_2O_3	P_2O_5	Reference
45S5	24.5	0	0	24.5	45	0	6	[59]
S53P4	23	0	0	20	53	0	4	[55]
13-93	6	12	5	20	53	0	4	[59]
13-93B1	5.8	11.7	4.9	19.5	34.4	19.9	3.8	[59]
13-93B3	5.5	11.1	4.6	18.5	0	56.6	3.7	[59]

Table 1-1: Table of relevant glass formations by weight percentage. The glass formulation to be studied in this work, 13-93B3, is highlighted.

1.4. Composition, Degradation, and Significance of Bioactive Glass 13-93B3

13-93B3 is a bioactive glass that contains six different oxides with various purposes. Boron trioxide (B_2O_3), the matrix, makes up more than half of the glass's weight (Table 1-1). As a supplement, boron also helps to promote cortical bone strength.[62] Boron has been found to dissolve faster from glass than silicon does, and in an *in vitro* physiological environment, borate glass was also found to convert more completely into hydroxyapatite than silicate glasses.[61] This dissolution process is assisted by sodium oxide (Na_2O) and potassium oxide (K_2O), which are network modifiers that break up the glass structure by influencing the boron network to contain BO_4 units alongside BO_3 units. Na and K are light alkali metals that are in turn hard acids, and these are able to stabilize the hard base BO_4 electrostatically.[63] The mixture of tetrahedral BO_4 and trigonal planar BO_3 units in B_2O_3 is less durable than the tetrahedral units that make up SiO_2, and so the borate-based 13-93B3 breaks down faster and more completely than glass with a tetrahedral silicate matrix does.[51,61,64] Calcium oxide (CaO) is also a network modifier. Both calcium oxide and phosphorus pentoxide (P_2O_5) contribute calcium and phosphorus ions, which make up calcium phosphate and lead to the formation of hydroxyapatite. Magnesium, added in the form of magnesium oxide (MgO), is another network modifier.[65] Magnesium also promotes bone remodeling and skeletal development, and magnesium deficiencies can cause bone fragility.[65,66] The maintenance of calcium levels in bone are partly facilitated by magnesium, and so magnesium helps to regulate bone density.[67] Magnesium also encourages the adhesion of osteoblasts (bone-building cells) upon surfaces through an integrin-mediated mechanism, which would help attach bone to 13-93B3.[68]

13-93B3 converts into hydroxyapatite when in a physiological solution, and this process takes several steps. First, Na^+ dissolves from the glass structure, and the solution breaks down the B-O bonds in the matrix.[61] Freed Ca^{2+} and PO_4^{3-} from the glass as well as PO_4^{3-} already in solution react to initially form amorphous calcium phosphate. Hydroxide (-OH) functional groups from the solution combine with the amorphous calcium phosphate layer, thus transforming the layer into hydroxyapatite. Carbonate (CO_3-) functional groups from the solution and magnesium ions from the reacting glass can also become incorporated, forming carbonated hydroxyapatite with magnesium substitutions for calcium in its molecular structure.[59,69] This non-stoichiometric hydroxyapatite would be similar to the type seen in natural bone, and this similarity can boost osteoconductivity when near living bone.[70]

While 13-93B3 may be able to function as an antibiotic carrier, bioactive glasses such as 13-93B3 are too brittle for any mechanical use on their own, much less for loading applications.[36,71] In order to prevent an infection next to a joint prosthetic, 13-93B3 would need to be supported by a tougher material, such as bone cement. If added to antibiotic-loaded bone cement to create a composite and placed in a solution, bioactive borate glass 13-93B3 would degrade and form pathways for antibiotics to leave the bone cement. 13-93B3's quality for attracting bone growth would also help integrate the bone cement with the body further and allow for the body's immune response to reach and eliminate bacteria before they can form biofilm footholds.

1.5. Conclusion

Antibiotic elution from PMMA-based bone cement is limited, and this is likely due to the occlusion of antibiotics in the cement. This low output wastes antibiotics and may give bacteria the opportunity to develop a resistance against the antibiotic. Adding a borate bioactive glass to antibiotic-loaded bone cement and allowing the glass to dissolve would create openings in the cement that would help release extra antibiotic material. The bioactive glass would also have the added effect of forming a hydroxyapatite-like material by providing calcium, phosphate, and magnesium into the solution that can precipitate back onto the bone cement's surface. This precipitate, which is osteoconductive, would encourage bone growth around the bone cement.[33] Integrating bone cement with living bone would reduce the open surface area on the cement that bacteria can potentially latch onto and help regenerate bone lost during surgery.

This work is meant to assess the suitability of commercial bone cement and borate bioactive glass 13-93B3 composites as a bone cement alternative with an increased capacity for potential antibiotic release and bone attachment. This study combines 13-93B3 glass particles with SmartSet MV in various loading amounts and particle sizes and covers the following three chapters. Chapter 2 characterizes the mechanical strength of the composites before and after soaking in a saline solution by measuring the compressive strength and Young's moduli of the samples and comparing these values to a control of bone cement containing no glass. The weight loss and water uptake of the samples were also measured to gauge the progression of glass degradation and to see how much water was entering the composites, which may reduce mechanical strength but also increase the transport of material out of the composites. The extent of the glass degradation was also measured using solution pH and ionic concentrations. Chapter 3 encompasses work studying the morphology and identity of the white precipitate that accumulated on the pellet surfaces over time. This was done using SEM to view the morphology of the precipitate, and three spectroscopy techniques (electron dispersive spectroscopy, Fourier transform infrared spectroscopy – attenuated total reflection, and micro-Raman spectroscopy) were used to identify the elements and molecular bonds in the material. Overall conclusions and potential future directions for this work are discussed in Chapter 4.

Chapter 2: Characterization of the Degradation of Bone Cement and Boron-Based Bioactive Glass Composites

2.1: Abstract

Bone cement is used to fill gaps and attach prostheses to bone. Adding a resorbable bioactive glass to antibiotic-loaded commercial bone cements would potentially offer a means to increase drug elution while promoting local bone formation. This study characterizes the mechanical and degradation properties of composites containing commercial bone cement and the borate bioactive glass formulation 13-93B3, which can dissolve in physiological fluid. Here, 5 µm, 33 µm, and 100 µm-diameter glass particles were each mixed with bone cement to create 20%, 30%, and 40% glass-loaded mixtures. Mixtures and controls were soaked in phosphate-buffered saline (PBS). Compressive strength, Young's modulus, weight loss, water uptake, solution pH, and ionic concentrations were measured for each group per soak duration. Compressive strengths of glass-loaded samples decreased over time but remained higher than the minimum ASTM standard of 70 MPa. The average Young's modulus of the composites did not exceed 3 GPa. Weight loss and water uptake of samples did not extend beyond 2% and 6%, respectively. The pH and boron concentration of all solutions increased over time, and a higher percentage of glass loading resulted in a higher pH. Increases in pH and boron concentrations indicated that more glass converted into water-soluble alkaline products, such as NaOH. The composites used in this study showed signs of glass degradation without compromising their mechanical strength to the point of ineffectiveness. Future studies can examine the effects of incorporating antibiotics such as vancomycin into the composites and determine if the composites meet other ASTM standards for acrylic bone cement.

2.2: Introduction

Bone cement is a material used by surgeons to fill gaps in bone and around metal implants placed into joints. Commercial bone cement is primarily made of poly(methyl methacrylate), or PMMA, and fillers are added to bone cement to initiate polymer polymerization, to increase the radiopacity of the cement, and to increase its shelf life.[16] One downside of bone cement is that this material can provide a place of attachment for the biofilms of infectious bacteria.[72] Systemic antibiotics can be given intravenously as an extra layer of prophylaxis, but the concentration of antibiotics at the surgical site from this method alone may be too low to fight bacteria off and may be toxic to other areas of the body.[73] Delivering antibiotics locally instead can introduce high amounts of antibiotics that can kill bacteria that would otherwise be resistant to lower systemic antibiotic concentrations, and this delivery system can also introduce antibiotics into avascular areas that are not accessible to systemic antibiotics.[74] bone cement is routinely mixed with antibiotics to combat bacteria in this way, but some of the antibiotics become trapped in the PMMA matrix and do not leave the cement, which wastes material.[15,28]

Despite this, in 1995, 90% of orthopedic surgeons manually added antibiotics to bone cement to prevent infections, and by 2004, several premixed low-dose antibiotic cements had been approved by the FDA for use in the second stage of a two-stage revision after the infection had cleared.[27,30] The release method of antibiotics from bone cement has been under debate, but the general consensus is that the release mechanism is a surface phenomenon.[31] After an antibiotic-loaded bone cement is immersed in a liquid, an initial release burst of antibiotics at the surface of the bone cement occurs, followed by a longer release of low amounts of antibiotics.[32] This amount may be too low to inhibit the growth of bacteria and may instead allow resident bacteria to develop a resistance, rendering the antibiotic ineffective and requiring a different method to clear out the infection.[26]

Beads of antibiotic-loaded PMMA have been used clinically to locally deliver antibiotics to a joint. However, these beads are normally removed surgically soon after implantation to prevent release rates that are too low to fight bacteria.[41,75] In one study, only 35% of the antibiotics inside commercial Septopal beads (Biomet Merck, Darmstadt, Germany) were found to have eluted after 45 days.[28] In another study, routine culture tests showed that PMMA beads loaded with gentamicin appeared to eradicate bacteria in patients, but Neut et al. discovered through more rigorous laboratory testing and scanning electron microscopy (SEM) that the PMMA beads were covered with bacteria.[76] They later discovered a clinical case of gentamicin-loaded beads still eluting gentamicin in a patient five years after implantation.[41] Tunney et al. also discovered gentamicin-resistant bacteria on infected hip implants that were cemented using gentamicin-loaded bone cement.[25] These findings suggest that the eventual sub-inhibitory release rate of antibiotic-loaded bone cement could allow for infectious bacteria to develop a resistance against the antibiotic and flourish again.

As composites, acrylic bone cement has previously been combined with bioactive glasses in literature, and this is usually meant to improve the cement’s bone-binding ability and its mechanical properties. Bioactive glasses are materials that can degrade in a physiological solution and release ions helpful for bone growth.[57] While these glasses can potentially increase antibiotic release from bone cement by creating pores, adding a new material such a dissolvable glass can affect the mechanical integrity of the bone cement, and so its mechanical properties should be watched. In literature, adding bioactive glass to PMMA does not seem to initially weaken the PMMA, however. Shinzato et al. added a silicate-based bioactive glass with average particle diameter ranges of 4, 5, 9, and 13 µm to PMMA and tested the glass's effect upon the cement's mechanical properties and osetoconductivity.[77] They found that cement composites with smaller glass particle sizes had higher bending strengths and a higher affinity to bone than did composites with larger glass particles. The same group also tested the effect of glass loading amounts of 40%-70% upon the mechanical strength of PMMA, and increases in the loading amount correlated with increases in the bending strength and bone affinity of the cement.[78,79] PMMA has also been mixed with both bioactive glass and antibiotics and studied in the past. Arcos et al. added gentamicin sulfate to a mixture of a silicate-based glass and PMMA and determined that the addition of PMMA and antibiotics did not affect the bone-binding ability of the glass.[80] Fernández et al. found that adding 60-70 wt.% phosphate-based glass to PMMA increased the amount of vancomycin released from the cement.[81]

While bioactive glasses have been mixed into PMMA before, the interactions between bioactive glass 13-93B3 (mol%: 6 Na_2O, 7.9 K_2O, 7.7 MgO, 22.1 CaO, 54.6 B_2O_3, 1.7 P_2O_5) and a PMMA-based cement have not been studied. Like other bioactive glasses, 13-93B3 can dissolve and convert into a hydroxyapatite-like substance over time within the human body's environment. Borate glasses such as 13-93B3 differ from more common silicate-based bioactive glasses, however, by degrading faster and more completely.[61] 13-93B3's main elemental component is boron, which make up the matrix in the form of B_2O_3. This glass also contains potassium and sodium, which help to break up the matrix for quicker dissolution. Calcium and phosphorous in the glass contribute the building blocks of calcium phosphate and hydroxyapatite. Magnesium, an element that assists with bone growth, is also included.[65]

If 13-93B3 is mixed into bone cement and encounters a physiological fluid, then this glass can dissolve and create openings in the cement, allowing a way for antibiotics within the cement to enter the solution. This added porosity of the cement would potentially increase the amount of antibiotic delivery.[82] Because of its fast-acting and thorough degradation, 13-93B3 incorporated into the commercial bone cement could be able to both deliver material at a joint for bone growth while creating pathways in the cement for extra future antibiotic elution.

This work characterizes the mechanical properties of composites of borate-based bioactive glass 13-93B3 and bone cement by measuring their compressive strengths and Young's moduli over time spent soaking in phosphate-buffered saline (PBS). Adding a biodegradable material into bone cement would create voids in the cement over time, which would allow for further elution of glass components and potentially antibiotics. However, this may decrease the mechanical strength of the cement to below the compressive strength ASTM standard of 70 MPa and cause the bone cement to become undesirable for weight-bearing applications.[40] Because of this standard, the compressive strength of the composites must be monitored. The Young's (elastic) modulus of the composites is also important to assess because an implant with a modulus considerably higher than the modulus of interfacing bone can cause the bone to degrade due to stress shielding.[83] The Young's modulus of cortical bone and cancellous bone is 3-30 GPa and 200-500 MPa, respectively, and in one canine study, the use of a bone cement with a Young's modulus of 9.7 GPa caused bone reabsorption.[84,85] The weight loss and water uptake of the composites were also studied because these measures reflect the amount of water penetration into the pellets. Water uptake can negatively affect mechanical properties by degrading the bone cement itself, though some water uptake is needed to help transport glass material out of the composite.[15,18,86] pH and the ionic concentrations of B, Mg, and P were measured over time from the phosphate-buffered solutions that immersed the composites, as these also relate to the degradation of the bioactive glass. The glass components that enter the solution undergo hydrolysis through the following primary reactions: $Na_2O + H_2O \rightarrow 2NaOH$, $K_2O + H_2O \rightarrow 2KOH$, $MgO + H_2O \rightarrow Mg(OH)_2$, $CaO + H_2O \rightarrow Ca(OH)_2$, $B_2O_3 + 3H_2O \rightarrow H_3BO_3$, and $2P_2O_5 + 6H_2O \rightarrow H_3PO_4$. The first four products are strong bases, and the last two are weak acids. The strong bases would contribute hydroxide anions that elevate the solution pH. As the glass continues to dissolve, the pH will increase, and therefore pH can be used as an indicator of the progression of the degradation of the glass and its transportation into the solution.[55] The concentration of ions originating from the glass would also increase in solution as the glass degrades. Rises in boron concentration can be used to determine glass degradation, and this would be the ion of choice because calcium, phosphorus, and magnesium ions are more readily incorporated into precipitated compounds, and potassium and sodium would already exist in the PBS (phosphate-buffered saline) solution to be used.[87,88]

2.3. Materials and Methods

2.3.1. Materials

DePuy SmartSet MV (DePuy, Warsaw, IN) was used as the commercial bone cement. SmartSet MV is packaged with a liquid and a solid component that forms a cement when mixed together. The liquid is comprised of 98 wt.% methyl methacrylate with 75 ppm hydroquinone, a stabilizer for storage. The remainder is N,N-Dimethyl-p-toluidine, a curing activator.[6] The solid component is 67.05 wt.% poly(methyl methacrylate) monomer; 21.1 wt.% methyl methacrylate/styrene copolymer, a hydrophobic fatigue strengthener; 1.85 wt.% benzoyl peroxide, a polymerization initiator; and 10 wt.% barium sulfate, a radiopacifier that causes the bone cement to be visible in x-rays.[7,18,20] The methyl methacrylate monomer in the liquid reacts with the powder PMMA in the solid component through free radical polymerization to form bone cement.

Bioactive glass particles were obtained from Dr. Mohamed Rahaman from Missouri University of Science and Technology. Glass with the formulation of 13-93B3 (mol%: 6 Na_2O, 7.9 K_2O, 7.7 MgO, 22.1 CaO, 54.6 B_2O_3, 1.7 P_2O_5) was prepared by mixing Na_2CO_3, K_2CO_3, $MgCO_3$, $CaCO_3$, $NaH_2PO_4 \cdot 2H_2O$, and H_3BO_3 (Fisher Scientific) together and heating the mixture at 1100°C for 1 hour inside of a platinum crucible. The material was then quenched between cold steel plates.

Three particle sizes of glass were prepared and designated as 5 µm, 33 µm, and 100 µm. The 5 µm size was used because this diameter is within a range often seen in literature.[44,53,57,79,89] 100 µm particles were also used because some studies have used glass particles >100 µm and because resultant pores with a diameter of at least 100 µm would allow for better tissue ingrowth.[61,90,91] The medium size, 33 µm, was picked by the recommendation of Dr. Mohamed Rahaman for having a glass surface area in between the surface areas of 5 µm and 100 µm glass particles.

To prepare the 100 µm glass, 200 grams of glass frits were weighed and ground for 30 seconds in a steel shatterbox (8500 Shatterbox, Spex SamplePrep LL, Metuchen, NJ). The glass was then sieved through stainless steel sieves, leading to a range of particle sizes between 75 µm and 106 µm. To create the 33 µm size, 100g of glass frits were weighed and ground for 150 seconds in the steel shatterbox. Through particle size analysis (Microtrac S3000 particle size analyzer), the glass was found to have an average size of 33 µm with a standard deviation of 19 µm. The 5 µm size was created by weighing and grinding 100 grams of glass frits for 150 seconds in the steel shatterbox. The glass was then additionally ground for 90 minutes in an attrition mill (Model 01-HD, Union Process, Akron, OH), using high-purity Y_2O_3-stabilized ZrO_2 as the milling media and ethanol as the solvent. Once dry, the glass was lightly ground with a mortar and pestle and then sieved though a 106 µm stainless steel sieve. Particle analysis determined that the glass had a particle size of 5 µm with a standard deviation of 3 µm. The particles were prepared at Mo-Sci Corp. (Rolla, MO).

The solution used in the following experiments was phosphate-buffered saline, which is also known as PBS (Ricca Chemical Company). PBS is an isotonic solution used in biological research.[18] Table 2-1 provides the weight percentages of components in the PBS solution used.

Component	H_2O	NaCl	Na_2HPO_4	KH_2PO_4	KCl
wt.%	99.02	0.08	0.14	0.03	0.02

Table 2-1: The composition of the PBS formula used.

2.3.2. Methods

2.3.2.1. Cement preparation

To create pellet samples, the solid component of the bone cement was poured into a bone cement mixing bowl that was connected to a vacuum source. Powdered 13-93B3 glass was then added to the bowl and mixed with the bone cement powder. The liquid bone cement component was then added, and the bowl was closed with a lid. The vacuum source was turned on, and the cement was mixed at 1 Hz for 90 seconds. Afterwards, the vacuum source was turned off and the lid was then opened, and the cement was then touched with a gloved finger to check the consistency of the cement. The cement was mixed in air with a spatula for 15 more seconds, after which the cement consistency was checked again. The doughing time was defined as the length of time between the beginning of the mixing and when the dough no longer formed strands when touched by a gloved finger.

After reaching doughing time, the cement was then pressed into polytetrafluoroethylene (PTFE) molds to form cylinders 12 mm tall with diameters of 6 mm. A PTFE plate was placed under the mold and the cement was pressed into the molds. Another PTFE plate was placed over the molds, and the plates were held in place around the mold using a C-clamp. The mold was then placed inside an incubator with a temperature of 37°C for one hour.

Afterwards, the bone cement pellets were pressed out of the molds and weighed. The pellets were then individually placed into 15-mL polypropylene tubes containing 2.5 mL PBS. After 0, 1, 3, 7, and 21 days of soaking, the pellets were removed from the PBS and further tested upon.

Ten different compositions of glass-incorporated bone cement were made, and their formulations and name designations are listed in Table 2-2. The percentages in their names are the percentages of glass that composed the dry material (SmartSet MV powder with glass) before becoming mixed with the liquid component. Glass loading amounts of 20%, 30%, and 40% were used because these were moderate values within the range used in literature. In studies of bioactive glass and bone cement composites, glass loading amounts have ranged from 4% to as high as a total wt.% of 70%.[78,92]

Sample Group	Glass Loading (wt.%)	SmartSet MV Powder (g)	Glass (g)	Liquid Component (g)	Glass Component (wt.%)
Control	0	40	0	18.88	0
20% 5 µm	20	40	10	18.88	14.5
30% 5 µm	30	40	17.14	18.88	22.5
40% 5 µm	40	40	26.67	18.88	31.2
20% 33 µm	20	40	10	18.88	14.5
30% 33 µm	30	40	17.14	18.88	22.5
40% 33 µm	40	40	26.67	18.88	31.2
20% 100 µm	20	40	10	18.88	14.5
30% 100 µm	30	40	17.14	18.88	22.5
40% 100 µm	40	40	26.67	18.88	31.2

Table 2-2: The mixing compositions of the glass-loaded bone cement groups used.

2.3.2.2. Mechanical Testing

Using an MTS Mini Bionix 858 load frame (MTS Systems Corporation, 14000 Technology Drive, Eden Prairie, MN), the compressive strengths of unsoaked samples were tested 24 ± 2 hours from the beginning of mixing time as well as after 1, 3, 7, and 21 days of soaking. Samples were crushed at a loading rate of 20 mm/min to either 40% strain or at fracture, whichever occurred first. Here, fracture was considered to have occurred when the loading fell to 90% of its peak value. The compressive strength of the pellets is the failure load divided by the cross-sectional area of the pellets. ASTM F451 defines the failure load as the load at the 2.0% offset from the elastic section of the stress-strain curve, the ultimate yield load, or the load at fracture, whichever occurred first. The ASTM F451 and ISO 5833 standard for the compressive strength of acrylic bone cement is a minimum of 70 MPa after 24 ± 2 hours from the beginning of cement mixing.[40,93] Glass mixtures were paired with controls that were tested at the same time. Five samples were tested from each group except where noted.

Young’s modulus is the elastic stiffness of a sample and is numerically the slope of the elastic section of a sample’s stress-strain curve. This value was collected alongside the compressive strength by MTS Series 793™ Control Software (MTS Systems Corporation, 14000 Technology Drive, Eden Prairie, MN) at 20 Hz.

2.3.2.3. Water Uptake

After soaking in PBS for a designated amount of time, pellets were removed from the solution with tweezers and rinsed with deionized water to remove excess PBS from the pellet surfaces. The pellets were then blotted with KimWipes (Kimberly-Clark, Irving, TX) and weighed. The water uptakes of the pellets were calculated using the following equation:

$$Water\ Uptake = \left(\frac{m_{final} - m_{initial}}{m_{initial}}\right) x\ 100\%$$

where $m_{initial}$ is the initial weight of the pellet after being removed from the molds, and m_{final} is the weight of the pellet after being rinsed in deionized water. This experiment was performed in triplicate, and glass mixtures were paired with controls that were tested at the same time.

2.3.2.4. Weight Loss

After the water uptake of the pellets were measured, the pellets were placed in histological glass jars, which were then placed on an autoclave tray and kept in an oven set to 90°C. After one day, the pellets were weighed again. The weight losses of the pellets were calculated using this equation:

$$Weight\ Loss = \left(\frac{m_{dry} - m_{initial}}{m_{initial}}\right) x\ 100\%$$

where $m_{initial}$ is the weight of the pellet after being removed from molds, and m_{dry} is the weight of the pellets after being taken out of the oven. This experiment was performed in triplicate with the same samples studied for their water uptake.

2.3.2.5. pH and Ionic Concentration

The pH values of the solutions were found by combining the solutions from three pellets and recording the pH of the combined solutions with a Fisher Scientific accumet™ AB15 Basic (Thermo Fisher Scientific, Waltham, MA) pH meter.

To gather ionic concentration data, the solutions that were used with the pellets for weight loss and water uptake tests were diluted with water and nitric acid to become a 2 v/v% nitric acid solution. This was analyzed with ICP-OES using a Jobin-Yvon JY 138 Ultrace (Horiba Jobin Yvon, Inc., 3880 Park Ave, Edison, NJ). To dilute the solutions, 2.5 mL of 2 M nitric acid was added to the vial of each sample solution. The mixture was then vortexed. Afterwards, 1.6 mL of the mixture was added to 30.2 mL of DI water in a 50-mL vial. Then, 8.2 mL of 2 v/v% nitric acid was slowly added. A sample of diluted PBS was used as the Day 0 reading for the ionic concentrations in each group. This experiment was performed in duplicate except for 20% 100 µm, which does not have a Day 1 and has a sample size of n=1 for Day 22. Ionic concentrations were not collected for 33 µm samples due to limited equipment availability.

The magnesium concentrations relative to the boron concentrations in solution over time were computed for the groups tested. This ratio was normalized to the magnesium-to-boron weight ratio in 13-93B3’s formulation (15.78%). For this comparison, Day 0 concentrations were subtracted from the data so that only magnesium and boron originating from the glass was represented. If the glass dissolved congruently and remained in solution, meaning that the relative amounts of boron and magnesium that dissolved were the same as their proportional amounts in the glass, then the ratio would have a value of one. A value greater than one would mean that more magnesium was in solution than would be expected based on the amount of boron in solution, and a value less than one would mean that less magnesium is in solution than would be expected from the boron concentration.

2.3.2.6. Statistical Analysis

To perform statistical analysis upon the pellets for compressive strength, Young’s modulus, weight loss, and water uptake, composites and controls tested at the same time were treated as separate blocks and were compared against each other. This was done to control for environmental variability that would otherwise confound the results, as different composite groups were tested on different days. To increase graph readability, the shown control data for each day in Figures 2-1, 2-2, 2-3, and 2-4 was the result of combining the controls for all loading amounts. See the appendix for the extended versions of these figures which show all composite and control comparisons.

The ± 1 sample standard deviation of each group is shown in the data where possible. Levene’s test was performed to check the equality of variances between glass-bone cement composites and their respective controls. Unpaired t-tests were then performed upon the compressive strength, modulus, weight loss, and water uptake data with equal variance. Comparisons involving unequal variances were made using Welch’s t-test. Composites were considered significantly different from their respective controls if $p < 0.05$. The analysis was performed using MATLAB (The Mathworks, Inc., Natick, MA).

A propagation of uncertainty calculation was performed to report the ± 1 standard deviations of the ratios of the ionic concentrations of magnesium and boron over time:

$$\mathrm{s}_{\frac{Mg}{B}} = \sqrt{\left(\frac{\partial \frac{Mg}{B}}{\partial Mg}\right)^2 \left(\mathrm{s}_{Mg}\right)^2 + \left(\frac{\partial \frac{Mg}{B}}{\partial B}\right)^2 (\mathrm{s}_B)^2} = \sqrt{\frac{1}{B^2}\left(\mathrm{s}_{Mg}\right)^2 + \frac{Mg^2}{B^4}\,(\mathrm{s}_B)^2}$$

where “s” is the sample standard deviation and “Mg” and “B” are the concentrations of magnesium and boron, respectively.

2.4. Results

2.4.1. Compressive Strength

The compressive strengths of the composites and the controls after various soaking durations are shown in Figure 2-1. In all cases, the compressive strengths of the samples did not fall below 70 MPa. When significantly different from their respective controls, 5 μm glass composites had a higher compressive strength than the control, and 33 μm and 100 μm glass composites had lower average compressive strengths than their controls. Increasing the loading amount of 5 μm glass appeared to raise the compressive strength of the glass, while increases in the amount of 100 μm glass lowered the compressive strength. The 40% 33 μm group for three days of soaking had a sample size of n=4 due to a deficit of well-formed samples. The last 30% 5 μm group soaked for 20 days instead of 21 days because of a temporary logistical issue.

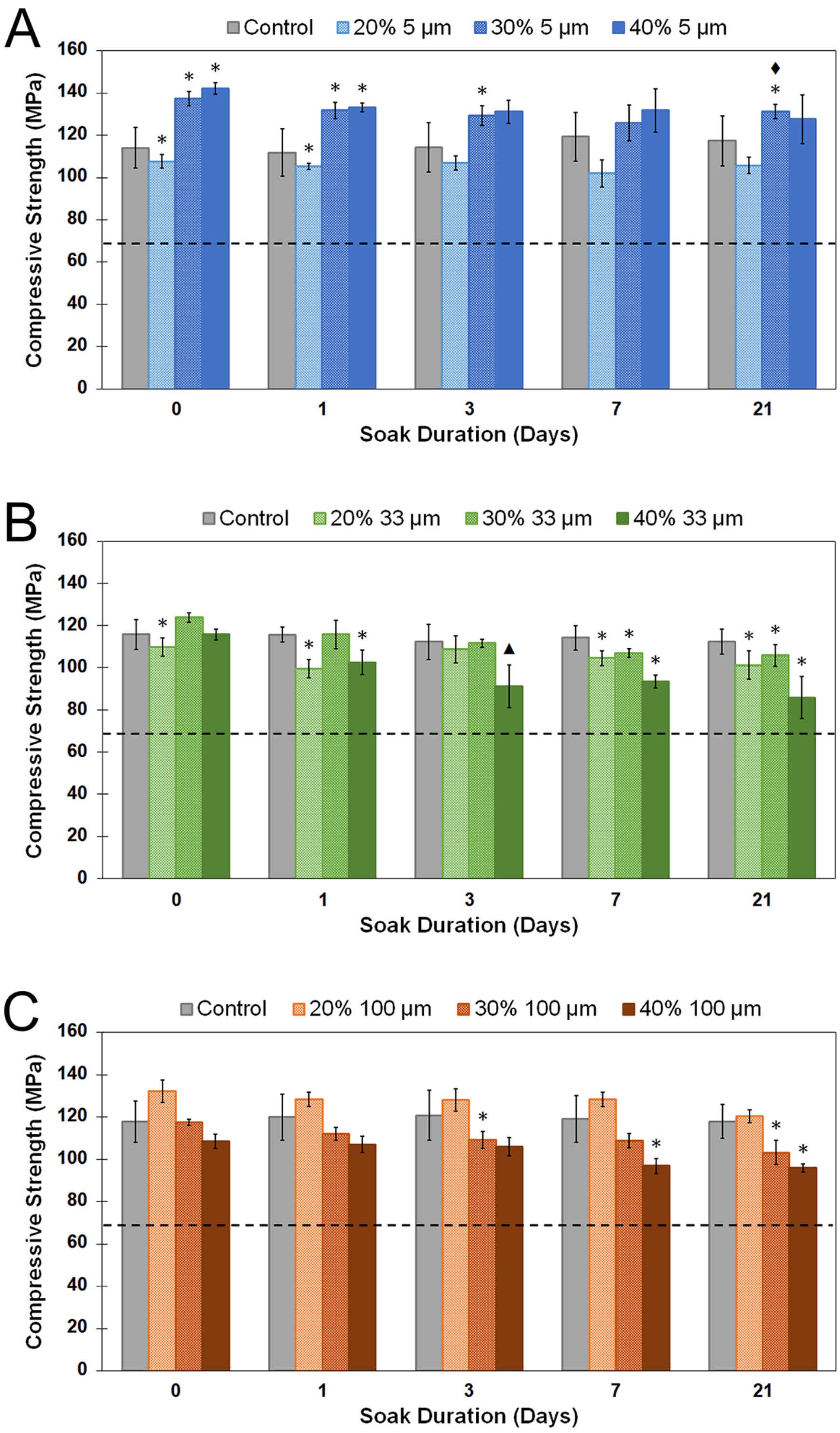

Figure 2-1: The compressive strengths of 5 µm (A), 33 µm (B), and 100 µm (C) composites and their respective cement controls. The control is the average of all controls tested at each time duration (n=15). The lines intersecting the graphs correspond to 70 MPa, the minimum standard from ASTM F451 and ISO 5833. A diamond (♦) represents a group that soaked for 20 days. A triangle (▲) represents a group of n=4. An asterisk (*) represents a significant difference ($p<0.05$) from the control set (n=5) that each group (n=5) was tested against (not shown).

2.4.2. Young’s Modulus

Figure 2-2 shows the Young’s modulus of the composites and the controls after soaking. When significantly different from their respective controls, 5 µm glass composites had higher moduli than their respective controls, and 33 µm and 100 µm glass composites had lower moduli than their control counterparts. The moduli of samples slightly decreased over soak time, and the averages decreased more over soak time as the loading amount was raised. The highest average Young’s modulus value, which was for 30% 5 µm without soaking, did not go beyond 3%.

Young’s modulus was collected from the same pellets used to record compressive strength, and so the 40% 33 µm group after three days of soaking had a sample size of n=4 and the final 30% 5 µm group soaked for 20 days instead of 21 days.

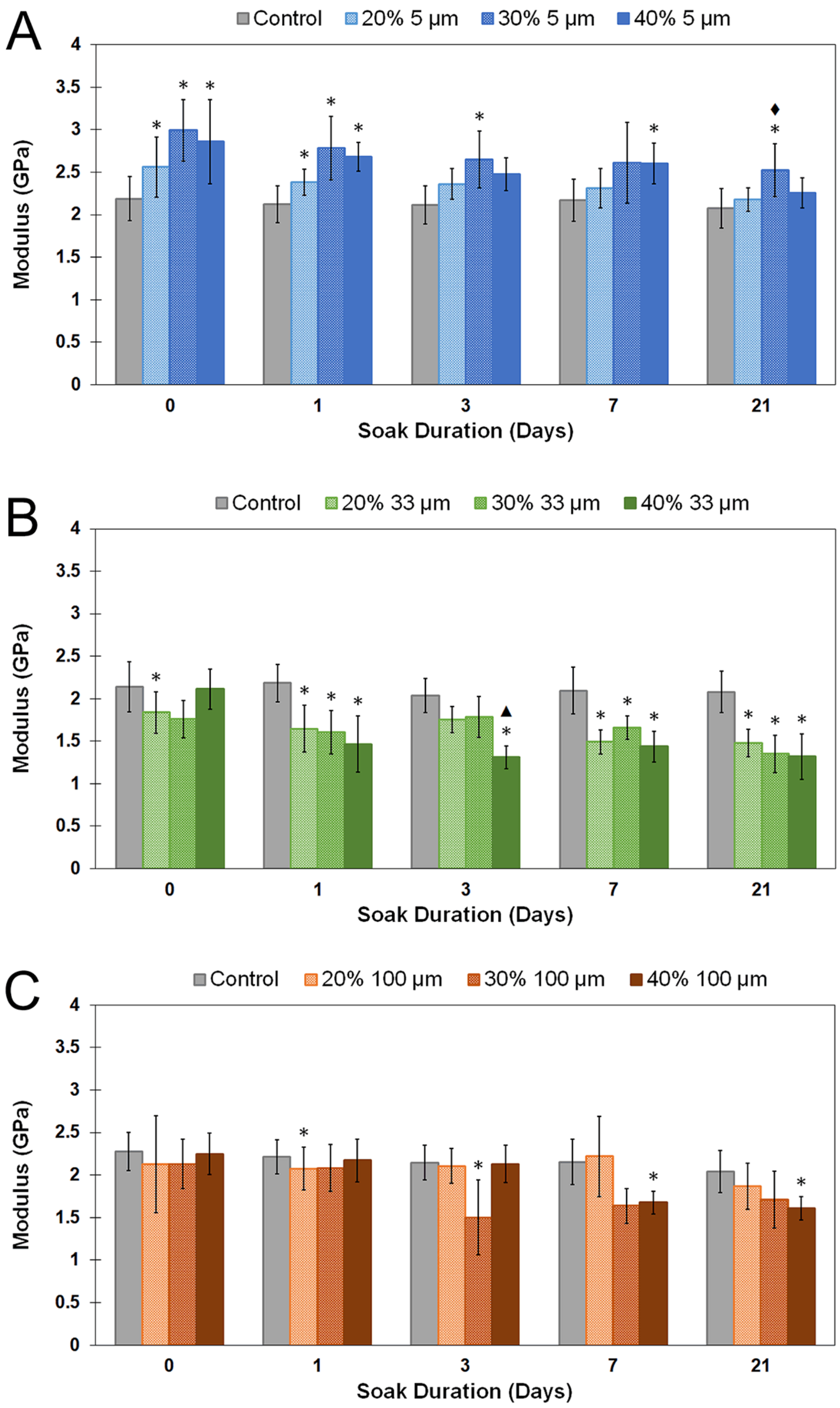

Figure 2-2: The Young's modulus of 5 µm (A), 33 µm (B), and 100 µm (C) composites and their respective cement controls. The control is the average of all controls tested at each time duration (n=15). A diamond (♦) represents a group that soaked for 20 days. A triangle (▲) represents a group where n=4. An asterisk (*) represents a significant difference ($p<0.05$) from the control set (n=5) that each group (n=5) was tested against (not shown).

2.4.3. Weight Loss

Figure 2-3 shows that the weight loss of the control samples consistently stayed under 1% of their original weights after soaking and drying. All composites lost weight within the first week of soaking, but their average weight loss did not exceed 1.5% of their original weight. Some groups gained weight between 7 and 21 days, and these were the 33 µm groups and the 20% and 30% 5 µm groups. Whenever the composites were significantly different from the control, all composites except for 20% 33 µm samples had a lower weight loss than the control which had a higher average weight loss than the control.

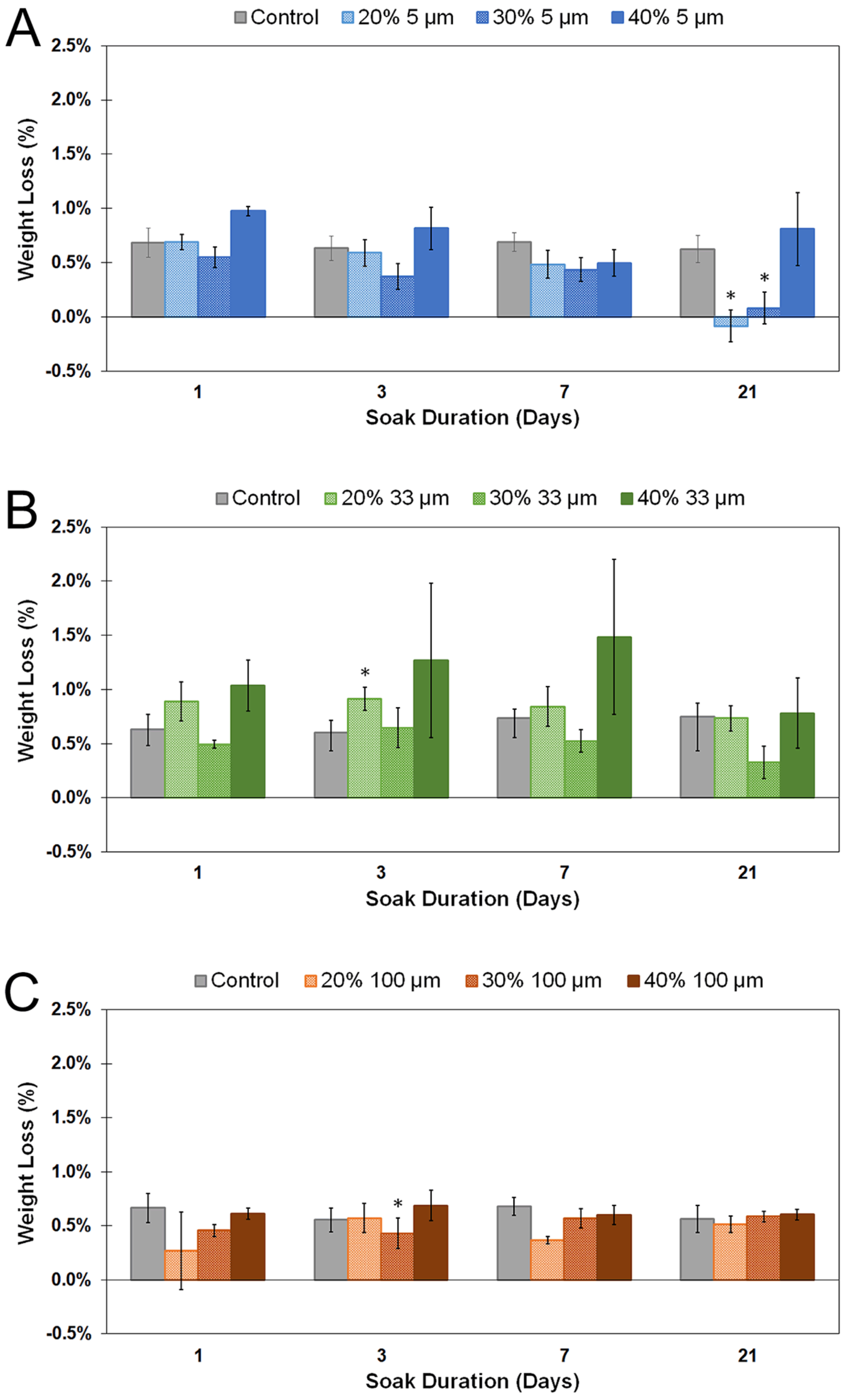

Figure 2-3: The weight loss of 5 µm (A), 33 µm (B), and 100 µm (C) composites and their respective cement controls. The control is the average of all controls tested at each time duration (n=9). An asterisk (*) represents a significant difference ($p<0.05$) from the control set (n=3) that each group (n=3) was tested against (not shown).

2.4.4. Water Uptake

From the water uptake data seen in Figure 2-4, all composites retained more water than their control counterparts, and their average water uptake generally increased as soak time lengthened. For 33 µm and 100 µm composites, the 40% loaded version contained the most water after 21 days. 20% 100 µm was the only group to not uptake a significantly higher amount of water than its respective control did throughout the experiment.

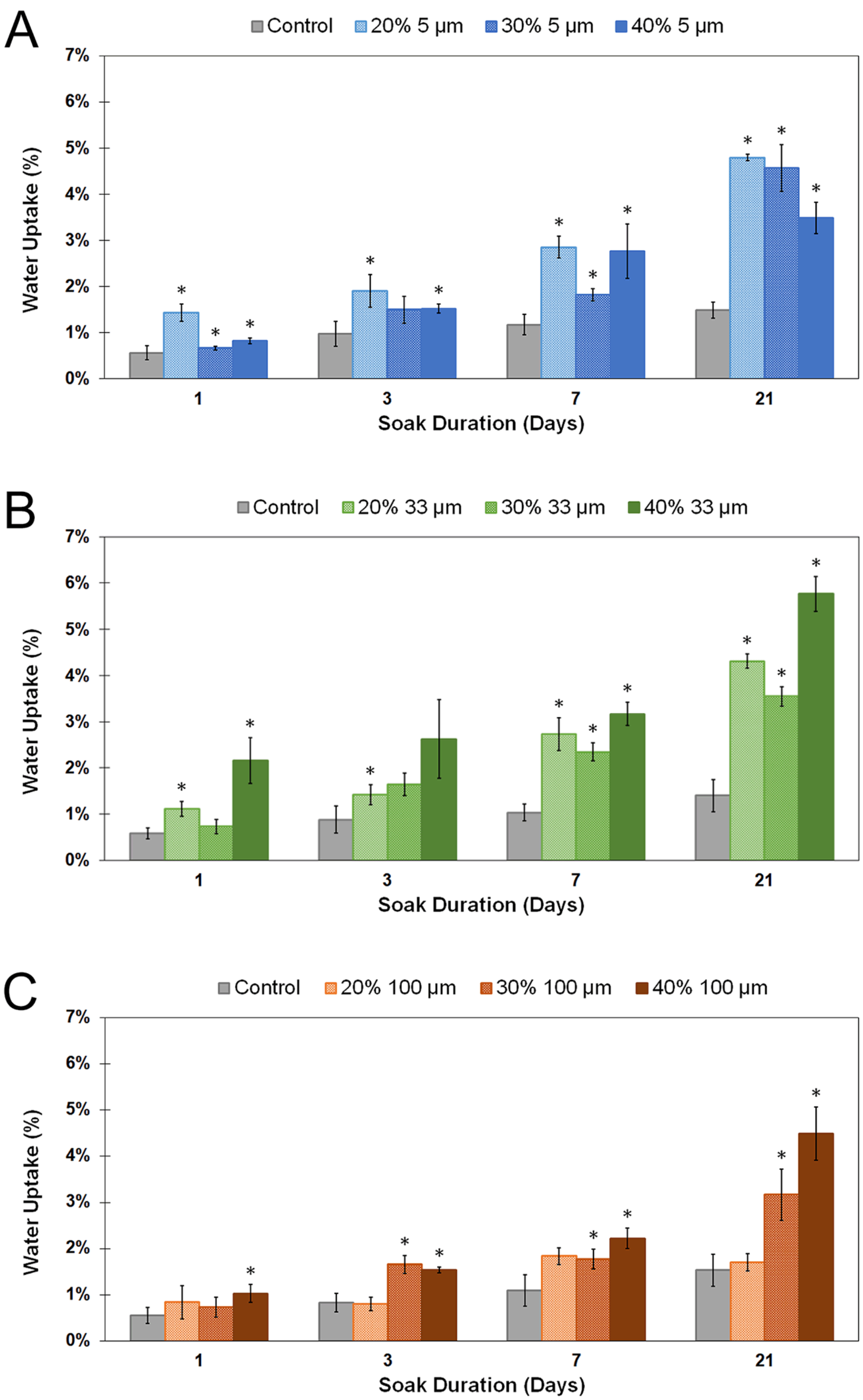

Figure 2-4: The water uptake of 5 µm (A), 33 µm (B), and 100 µm (C) composites and their respective cement controls. The control is the average of all controls tested at each time duration (n=9). An asterisk (*) represents a significant difference ($p<0.05$) from the control set (n=3) that each group (n=3) was tested against (not shown).

2.4.5. pH

The pH of the solutions were collected and shown in Figure 2-5. The pH values increased as the amount of glass increased and as the particle diameter size decreased. For solutions containing controls, the pH decreased slightly over time. The control values shown in Figure 2-5 were recorded at the same time that the 20% 5 µm group was recorded.

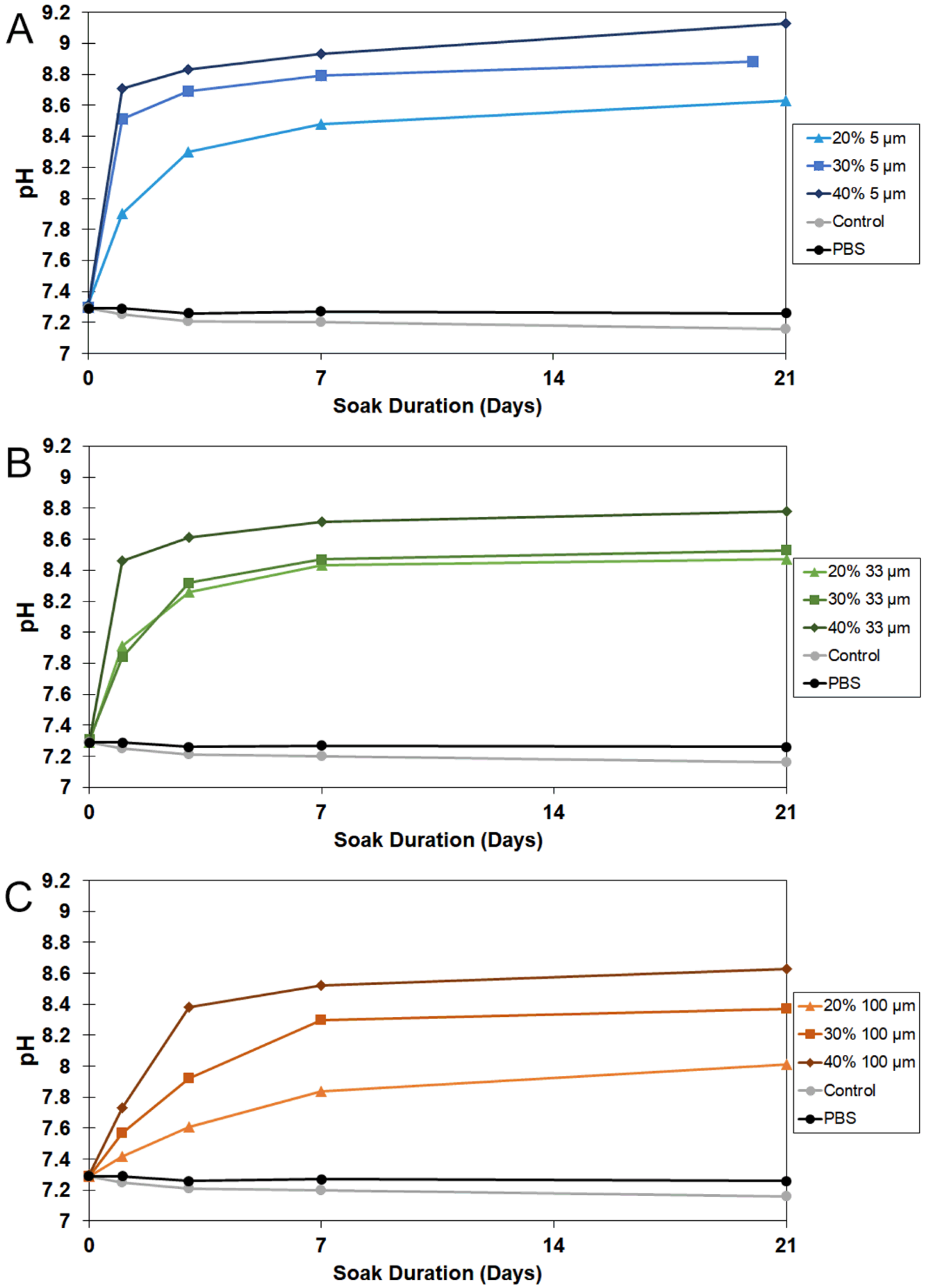

Figure 2-5: The pH of solutions for composites containing 5 µm (A), 33 µm (B), and 100 µm glass (C) with controls. The control and PBS values were collected at the same time the 20% 25 µm values were collected.

2.4.6. Ionic Concentration

The concentration of boron in solution increased as the glass particle size decreased and as the loading increased, which is shown in Figure 2-6. A higher glass loading appeared to increase the overall elution of boron. After 21 days, the difference between the boron concentrations from 30% and 40% glass mixtures were larger than the difference between 20% and 30% glass mixtures. For boron, 20% 5 µm had concentrations close to the concentrations of 40% 100 µm over time. The rates of boron and magnesium elution appeared to slow down over time, but more of both ions were still accumulating after 21 days, especially for 40% 5 µm.

Figure 2-7 shows the magnesium concentration relative to the boron concentration and normalized to the magnesium-to-boron weight ratio in 13-93B3's formulation. Less magnesium was in solution than would have been expected in a congruently-dissolving glass, and this was more pronounced for 5 µm groups.

The data for 20% 100 µm is shifted forward in time from the rest of the groups due to temporary logistics issues, and the ionic concentrations of calcium is not reported here due to recording errors. Composites containing 5 µm glass had lower Mg/B concentration ratios than composites with 100 µm glass. Composites with glass loading amounts of 40% also had the lowest Mg/B concentration ratios for their glass size.

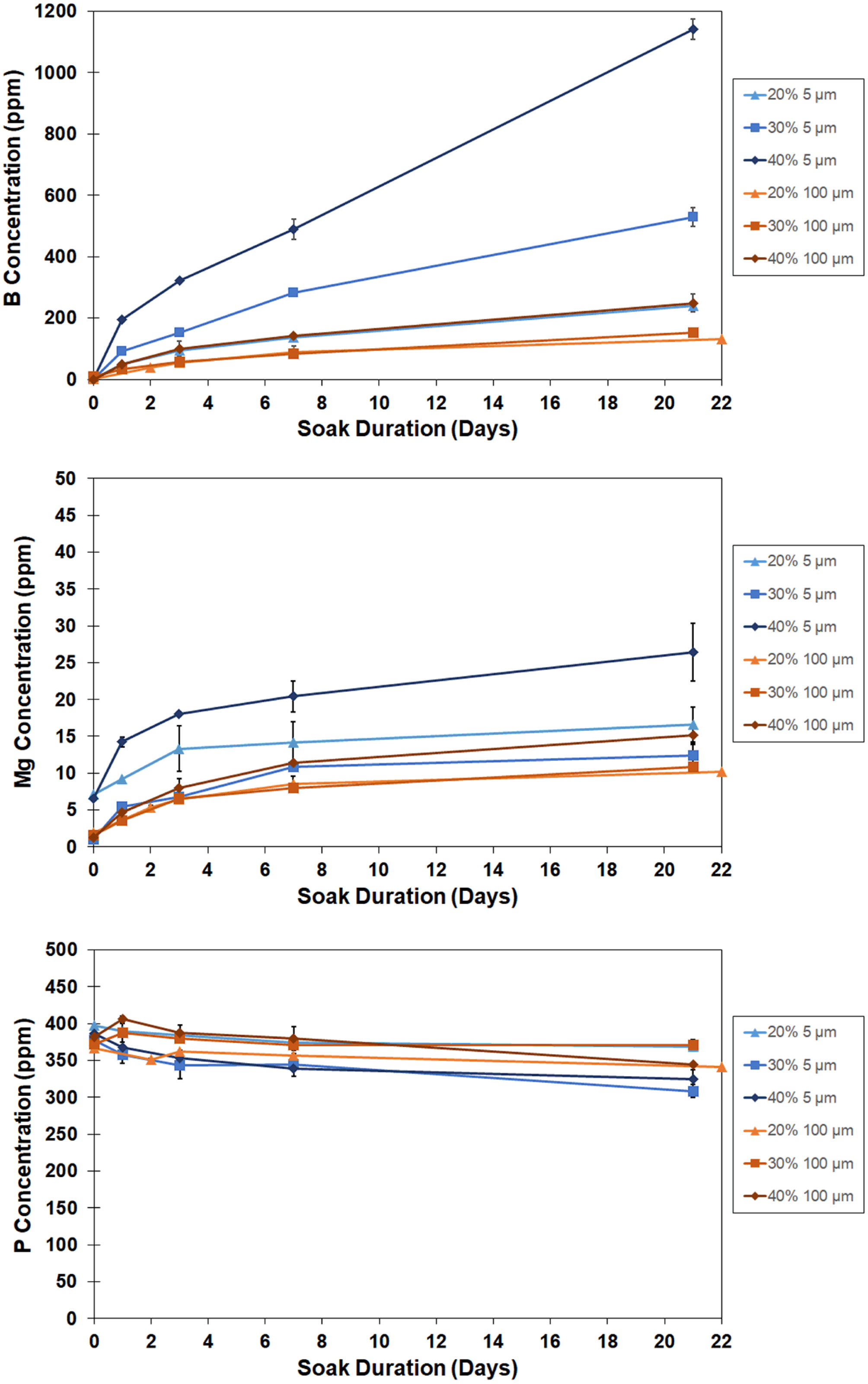

Figure 2-6: The ionic concentrations of B, Mg, and P over time in PBS (n=2). For 20% 100 µm, Day 2 is shown instead of Day 1, and the last data point (n=1) occurred at Day 22.

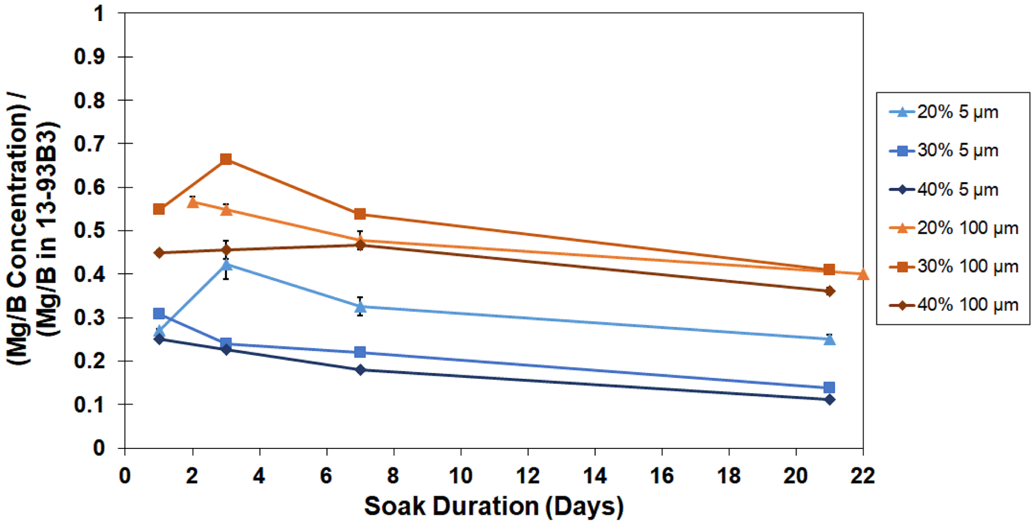

Figure 2-7: The Mg/B ratio of ionic concentrations over time in PBS, normalized to their original elemental weight ratio in 13-93B3 (n=2). For 20% 100 µm, Day 2 is shown instead of Day 1, and the last data point (n=1) occurred at Day 22.

2.5. Discussion

After the samples soaked in PBS, the composites with more than 20% glass loading showed signs of a white precipitate accumulating upon the surfaces while the controls did not look appreciably different from when they were cured. Therefore, physical changes to the composites over time due to the addition of the glass were visibly apparent.

Adding 13-93B3 particles to the PMMA strengthened the bone cement initially, but because the bioactive glass dissolved over time, the compressive strengths of the samples dropped as the soaking length increased. The decrease in compressive strength over time spent soaking was more evident for larger loading amounts. This was likely due to increased water penetration around the glass and because more glass was available to interact with the PBS. The same trend was seen for 100 µm composites. For 5 µm composites, the 30% and 40% glass loadings had a higher compressive strength than the control, while composites containing 33 µm particles had an initial average compressive strength less than the average of the control. This meant that the 33 µm glass size did not bond as well to the bone cement as the 5 µm composites did and therefore created areas of stress concentrations.[94] The lack of change in compressive strength for 20% 100 µm composites was most likely due to the low amount of glass surface area exposed to the PBS to undergo dissolution. The increase in compressive strength for 30% and 40% loadings of 5 µm glass after one day of soaking correlated well with the rise in strength seen by Shinzato et al., which used a silicate glass with an average particle size of 3.2 µm at those loading amounts.[79] The increases in the same groups seen with no soaking also correlated with the compressive strength rises in 30% and 40% borate glass-loaded PMMA documented by Lopes et al.[18]

The Young's moduli for the 5 µm composites was higher than the moduli of their respective controls, and this may have been because the 5 µm glass particles bonded well with the bone cement. The composites with larger particle sizes had lower moduli than their controls because their bigger size got in the way of the polymerization process.[95] As with the compressive strength, increases in the Young's modulus for 30% 5 µm and 40% 5 µm after one day of soaking relative to their controls followed the trend seen by Shinzato et al. for similar composites.[79] Because the borate glass dissolved while soaking, the Young's modulus typically dropped over time. This effect was increased for formulations with higher concentrations of glass, and this was likely because more glass was available to dissolve, causing a larger decrease in stiffness.

The Young's modulus of a suitable bone cement should be low enough to be similar to bone's modulus so that stress shielding does not occur around stiff implants and cause surrounding bone loss.[83] For comparison, the Young's modulus of cortical bone is 3-30 GPa, and the Young's modulus of cancellous bone is 200-500 MPa.[84] Composite moduli was approximately 1.5-3 GPa, which is between the moduli of cortical and cancellous bone and is less than the reported Young's modulus value to cause reabsorption.[85] Therefore, this suggests that the cement would not have a strong moduli mismatch issue with bone.

The average weight loss of pellets did not exceed 2%, which is similar to the weight losses seen in glass/PMMA composites previously reported by Lopes et al.[18] Notably, the weight losses seen in their work for PMMA, ~0.7%, is nearly identical to the values seen here for the bone cement control.[18] Increases in weight loss over time is likely due to the material in the glass leaching away from the pellet, and decreases in weight loss may be attributed to the accumulation of solid precipitate from the solution upon the pellet surface.[18] This cannot sufficiently explain the low weight loss seen in 20% and 30% 5 μm samples after 21 days of soaking, however. These pellets may have still contained water after the drying period, and a larger sample size would have made these readings more robust. Weight loss seen from the control could be from loose material detaching from the sample while soaking.

The average water uptake of the composites generally increased as soak time lengthened, meaning that the pellets were continually approaching but not reaching water saturation throughout the experiment. Therefore, water penetration into the pellets continually progressed over time past at least seven days.[18] Commercial bone cement has been shown to uptake water by less than 3 wt.%, and here water uptake did not exceed 6 wt.% for all composites.[18] An increased water uptake is correlated with a decrease in compressive strength, but this property may also cause the bone cement to expand and press into the surrounding implant and bone, stabilizing them further.[96] As predicted by the increase in water uptake, the compressive strength and Young's moduli of the composites did decrease over time spent soaking, but these drops were not enough to violate ASTM standards. As 13-93B3 is more hydrophilic than PMMA, composites containing more glass would be expected to absorb water and increase the water uptake as loading amount of glass in the pellet increased. The increased water uptake by the composite pellets as compared to the controls would also mean that more material could be moved out of the pellet by water transport.

The pH of the solutions rose as the glass particle diameter size decreased, which could be explained by the larger surface area of the smaller particles allowing for more interaction with the PBS and therefore quicker dissolution. 40% glass loadings consistently caused the highest pH values throughout the glass sizes, which was not surprising as more glass material would have been available for dissolution. The components that were released from the glass formed bases that would have increased the solution's pH as the glass eluted.[55]

Of the elements tested, boron consistently had the highest concentration in solution over time. This was expected because boron composes most of the glass and remains in solution without forming compounds with other elements, such as calcium and phosphorus. Increases in pH have been shown to increase the corrosion of borate bioactive glasses, and so the rise in boron concentration as the pH rose was anticipated.[97]

Magnesium concentrations also increased over time in solution, but compared to its relative concentration in the glass's formula to boron, less magnesium than would be anticipated had eluted from the composites. Borate glasses are assumed to dissolve congruently, and the most likely reason for the magnesium deficiency in the solution was due to its incorporation into the precipitate.[98] Notably, the magnesium product from degradation ($Mg(OH)_2$) is not soluble in water, which could cause magnesium to join the precipitate instead of the solution.[99] More magnesium came out of the solution for 5 µm samples than for 100 µm samples. This could mean that more precipitate formation was occurring in the 5 µm samples, which would provide more available material for magnesium to occupy. Likewise, the lower Mg/B ratio for 40%

loaded samples than for samples with less glass loading meant that 40% loaded samples underwent more precipitate formation.

The normalized Mg/B ratios seen in Figure 2-7 are lower than the ratios seen in one study testing 13-93B3 dissolution.[98] This is most likely because that study used a dynamic environment that prevented a buildup of ions, while here the samples remained in a static solution throughout the experiment. The lack of solution change would cause the magnesium in the solution to interact with the precipitate surfaces for longer, therefore causing more magnesium ions to become incorporated into the forming precipitate. In another study, however, even less magnesium relative to boron was seen in solution than here, and this discrepancy could be explained by the different glass composition and solution volume used.[99]

Phosphorus, despite being released from the glass, decreased in solution concentration over time because the phosphorus in solution was combining with the calcium dissolving from the glass to form calcium phosphate precipitates. As there was no calcium in the PBS (Table 2-1), calcium was the limiting reactant for precipitate formation.

2.6. Conclusion

Having either more glass available in the composite or incorporating glass in a smaller particle size appeared to cause higher glass dissolution, which raised the pH and boron concentrations and caused more precipitate to form. The mechanical properties of the cements tested here were not reduced enough to be considered unsuitable for loading applications. This suggests that the glass composites in this work could be used similarly to plain SmartSet MV while also providing material for bone growth and potential antibiotic delivery.

One limitation of the experimental design is that the samples were soaked *in vitro* without replacing the solution throughout the duration of the experiment. Therefore, this study more closely reflects the event that the glass's eluted material can accumulate in a space close to the samples. In an *in vivo* environment, the ions would be circulated away by the body, lessening the ionic concentrations and possibly increasing the degradation rate of the glass through Le Chatelier's principle.[58]

The samples used here were also vacuum-mixed during preparation to further control the physical properties of the pellets. Vacuum-mixing removes excess voids from the cement, and this was meant to minimize the chance that the cement would fall below the compressive strength ASTM standard; however, the compressive strengths of all composites studied were higher than the ASTM standard. Forming equivalent cement mixtures outside of a vacuum environment and testing them in the same way done in this work would investigate if cement with a higher porosity could also retain a compressive strength above 70 MPa. More of such pores would be advantageous for glass dissolution by allowing more water volume into the pellets and creating more exits for the glass's material, which would further increase the amount of material eluted.

Future directions include increasing the sample sizes for the experimental tests and lengthening the time points studied to see if the trends persist. The data here could be used to form a power analysis for the sample size in future work. More specifications in the ASTM F451 guidelines could also be tested, such as the maximum exothermic temperature of the composites when curing, the setting times of the composites, and the amount of residual monomer left after curing. ISO 5833 also has additional guidelines for the mechanical strength of acrylic bone cement that could be tested for these composites, such as a minimum bending strength of 50 MPa and a minimum bending modulus of 1800 MPa.

13-93B3 could be mixed with other commercial bone cements to test the effect of differing composite matrices, and antibiotics such as vancomycin and gentamicin can be added alongside 13-93B3 to see how this glass formulation affects their elution rate in cement. The amount and rate of antibiotic elution can be compared between composite groups and bone cement controls, and the effectiveness of the incorporated antibiotic at suppressing bacteria growth can be studied *in vitro*.

Chapter 3: Characterization of the Conversion of Bone Cement and Boron-Based Bioactive Glass Composites

3.1. Abstract

Borate bioactive glass 13-93B3 can convert into a hydroxyapatite-like material within the body, which can be helpful to attract bone growth around implants such as bone cement and prevent biofilm formation. In this study, 13-93B3 was incorporated into the commercial bone cement SmartSet MV, and the conversion of the glass into a precipitate was investigated with visual inspection via scanning electron microscopy (SEM) as well as with energy dispersive X-ray spectroscopy (EDS), Fourier transform infrared (spectroscopy) – attenuated total reflection (FTIR-ATR), and micro-Raman spectroscopy. Glass particles 5 µm, 33 µm, and 100 µm in diameter were each mixed with the commercial bone cement SmartSet MV to create 20%, 30%, and 40% glass-loaded mixtures. The precipitate that formed on the samples was found to be a calcium-deficient apatite partially substituted with magnesium ions, which would mimic bone material better than stoichiometric hydroxyapatite. Composites of bone cement and 13-93B3 show promise in encouraging bone formation on the surface of the bone cement, reducing areas where biofilms can form undetected by the body. Future studies could be carried out with bone cells *in vitro* and with bone *in vivo* to better simulate the human body's environment.

3.2. Introduction

Biofilms are extracellular structures made by bacteria to protect them from the environment, and their formation around a prosthetic joint implant is a health concern because of the difficulty of removing them using antibiotics.[24] When living in a biofilm, bacteria are up to a thousand times less susceptible to antibiotics than free-floating bacteria are.[33] If these have formed on the surface a prosthetic joint, the typical method of treatment is a joint revision surgery involving the removal of the implant along with surrounding bone and tissue.[5] This is financially costly and negatively affects the patient's quality of life by requiring further hospitalization and invasive procedures.[5]

Biofilms can form upon the surfaces of implanted material such as bone cement because some infectious bacteria, such as *Staphylococcus epidermidis*, are attracted to the hydrophobic nature of acrylic bone cement.[100,101] The patient's immune system can also have difficulty reaching the cement surface due to a lack of proper tissue adhesion to the cement, and this difficulty would be exacerbated by comorbidities that already hinder the immune system.[5,37,72] While loading antibiotics into implanted bone cement can temporarily suppress bacteria from the surrounding area, the initial strong release of antibiotics is short-lived.[28] Low concentrations of antibiotics eluted afterwards can allow bacteria to develop an antibiotic resistance and eventually colonize the bone cement.[32]

One potential way to combat biofilm formation is to use bioactive glasses, which have the ability to convert into hydroxyapatite that can attach to nearby tissues and attract growth from surrounding bone.[42,43] The first bioactive glass formulation devised was Bioglass 45S5, created by Dr. Larry Hench in 1969 at the University of Florida.[50] Another silicon-based bioactive glass formulation, 13-93, is more easily manufactured and is approved to be used *in vivo* in Europe.[52,53] 13-93B3 is a borate-based bioactive glass manufactured in Mo-Sci, Corp. in Rolla, Missouri, that is derived from the formulation of 13-93 and replaces the SiO_2 in the glass with B_2O_3 (Table 1-1).[52,61] The mixture of tetrahedral [BO_4] and trigonal planar [BO_3] units in B_2O_3 is less durable than the tetrahedral units that make up SiO_2, and so the borate-based 13-93B3 breaks down faster and more completely than glass with a silicate matrix does.[51,61,64]

13-93B3 is composed of six oxides (Table 1). Boron trioxide (B_2O_3) makes up the majority of the glass's weight. Boron has been found to dissolve faster than silicon from glass structures, and borate-based glass has also been found to react more completely in an *in vitro* physiological environment to convert into hydroxyapatite.[61] Degradation is assisted by sodium and potassium in the glass, which are network modifiers. Sodium and potassium are hard acids that can stabilize the hard base BO_4 electrostatically, and they break up the glass structure by encouraging BO_4 units to form in the boron network alongside BO_3 units.[63] This adds imperfections to the structure of the matrix, which reduces its durability.[51] Magnesium, another network modifier in the glass, is also an important element for bone growth and is added to 13-93B3 as magnesium oxide (MgO).[65] Calcium oxide (CaO) is also a network modifier. Both calcium oxide and phosphorus pentoxide (P_2O_5) contribute calcium and phosphorus ions, which make up calcium phosphate and contribute to the formation of hydroxyapatite.

When 13-93B3 interacts with a physiological solution, Na^+ first dissolves from the glass structure, and the solution degrades the B-O bonds.[61] Ca^{2+} and PO_4^{3-} from the glass as well as PO_4^{3-} already in solution react to form a layer of amorphous calcium phosphate. Hydroxide anions (-OH) from the solution combines with the amorphous calcium phosphate layer to slowly crystallize the layer into hydroxyapatite. CO_3- from the solution and magnesium from the glass can also become incorporated, changing the hydroxyapatite into a non-stoichiometric form.[59,69] If 13-93B3 is incorporated into bone cement and used as a part of a joint replacement, then the resultant hydroxyapatite-like products from the glass would help integrate the cement with adjacent bone and foster bone growth. This would further attach the cement to bone and reduce exposed surface area on the cement that bacteria can latch onto and form antibiotic-resistant biofilms.[34,35,41] In one study, a silicate bioactive glass added to PMMA-based bone cement was able to counteract the disruptions that PMMA caused to bone formation, so there is already a precedent for the benefits of combining bioactive glass and PMMA for bone growth.[37] Kamimura et al. compared the interfacial tensile strength of rabbit bone and commercial bone cement with and without silicate-based bioactive glass beads after four weeks of implantation.[102] In their experiment, bone cement that contained glass was found to have a higher bone-bonding strength than regular bone cement did.

While the conversion of 13-93B3 scaffolds has already been studied in literature, mixing bone cement with 13-93B3 may affect the morphology and identity of the converted products.[69,71] This paper examines the precipitate that collected on the surfaces of composites of 13-93B3 and a commercial bone cement, DePuy SmartSet MV (DePuy, Warsaw, IN). The progression of the glass conversion will be visualized here using SEM, and the elemental and molecular character of the precipitate will be studied using several types of spectroscopy that report different information about the composition of the precipitate. EDS detects the relative amounts of elements at selected areas of samples. FTIR-ATR readings rely upon the change in the permanent dipole of a molecular bond, and Raman spectroscopy relies upon the change of the polarizability of bonds.[103] Because the last two spectroscopies report molecular vibrations using different techniques (infrared absorption and Raman scattering), peaks that are strong in micro-Raman spectroscopy may be weak in FTIR-ATR and vice versa, and so micro-Raman spectroscopy can be considered to be a technique complementary to FTIR-ATR.[103,104]

3.3. Materials and Methods

3.3.1. Materials

The pellets used in this chapter were made in the same way explained in Chapter 2 (2.3.1., 2.3.2.1.). However, the time points for soaking were truncated to 0, 7, and 21 days. Samples that soaked for 7 or 21 days were dried in an oven at 90°C for one day. Pellets were kept in histological glass jars sealed with Parafilm until used for the tests outlined in this chapter.

3.3.2. Methods

3.3.2.1. Scanning Electron Microscopy

Pellets from each group were sputter-coated with an 80:20 gold-palladium alloy and were then observed through SEM (Hitachi S-2700, Tokyo, Japan) equipped with a Quartz PCI digital capture (Quartz Imaging Corporation., Vancouver, Canada). Comparative pictures of the morphology of the reacted surfaces were taken with 150x and 1500x magnification with an accelerating voltage of 15 kV.

3.3.2.2. Energy Dispersive X-ray Spectroscopy

The atomic compositions of the pellet surfaces were observable through SEM (Tescan VEGA LMU, Brno, Czech Republic) equipped with EDS (Bruker Quantax XFlash 100, Billerica, MA). The accelerating voltage was 20 kV, and the working distance was 15 ± 1 mm. 20% 5 µm and 40% 5 µm pellets soaked for 21 days that showed evident precipitate formation were studied with this technique. Three EDS readings from each group were averaged to determine the atomic elemental proportions of the precipitate seen on each surface. EDS elemental mapping was also conducted upon the 20% 5 µm surface.

3.3.2.3. Fourier Transform Infrared Spectroscopy – Attenuated Total Reflection

FTIR-ATR (Fourier transform infrared (spectroscopy) – attenuated total reflection) was used to detect the molecular bonds present in samples using infrared spectra, and this technique was used because not enough precipitate formed on each sample to be able to be analyzed with transmission FTIR. A PerkinElmer Spectrum 400 FTIR Spectrometer (PerkinElmer, Waltham, MA) with a diamond GladiATR accessory (PIKE Technologies, Madison, WI) was used to measure this from the sample surfaces. Pellets were placed upon the diamond crystal on the ATR appliance with their smooth circular surface touching the crystal, and the pellets were pressed down to maximize the surface contact with the crystal and strengthen the reading. The crystal's diameter was 3mm. The spectra were captured within the wavelength range of 400-4000 cm^{-1} with a resolution of 4 cm^{-1}, and representative spectra were the result of averaging 64 scans. The ATR readings were corrected using PerkinElmer's Spectrum software, and a correction value of "1" was used to transform the spectra to become equivalent to transmission FTIR readings.

FTIR spectra were collected from all groups. The spectra for the cement control after 0 and 21 days of soaking was also collected, and the spectra of as-received 13-93B3 were collected using 5 µm-sized glass because that size would have the most surface area in contact with the crystal.

3.3.2.4. Micro-Raman Spectroscopy

A Horiba Jobin Yvon LabRam ARAMIS Micro-Raman microscope (Horiba, Kyoto, Japan) was used to collect Raman spectra of samples. To record spectra, a 623.81 nm HeNe laser was used in conjunction with a 10x microscope, and individual spectra samples were each collected for five seconds. The wavelength range studied was 400-1600 cm^{-1}, and eight spectra were averaged for each group. Spectra were collected from an unsoaked control, a control soaked for 7 days, as-received 100 µm glass particles, and 20% 5 µm, 40% 5 µm, 20% 100 µm, and 40% 100 µm samples soaked for 7 and 21 days. Spectra baselines were corrected by using the polyfit function in MATLAB (The Mathworks, Inc., Natick, MA) to fit a third-order polynomial to the spectra that was then subtracted.

3.4. Results

For pellets containing 100 µm glass particles, the glass at the surface changed into an opaque white color after soaking that contrasted with the darker and more translucent appearance of the bone cement control. For pellets containing glass particles with smaller diameters than 100 µm, the sides of the pellets became pitted and covered with white protrusions while soaking, which increased as the glass loading increased. Two photos of comparative examples, shown in Figure 3-1, were taken using a Canon EOS 7D (Canon, Tokyo, Japan).

Figure 3-1: Left: From left to right, a 30% 5 µm pellet, a 30% 33 µm pellet, a 30% 100 µm pellet, and a control pellet. The samples were soaked for 7 days and were dried in an oven at 90°C for one day. Right: From left to right, a 20% 33 µm pellet, a 30% 33 µm pellet, a 40% 33 µm pellet, and a control pellet. The samples were soaked for 21 days and dried in an oven at 90°C for one day.

3.4.1. Scanning Electron Microscopy

A spherical-textured surface could be seen on the micrographs of a control (Figure 3-2). This is a property of commercial PMMA-based bone cement. In the picture, beads of pre-polymerized methyl methacrylate/styrene co-polymers from SmartSet's dry powder component are covered by PMMA, which polymerized around the beads when the cement cured.[15,16,72] The white rounded flecks embedded in the surface is barium sulfate.

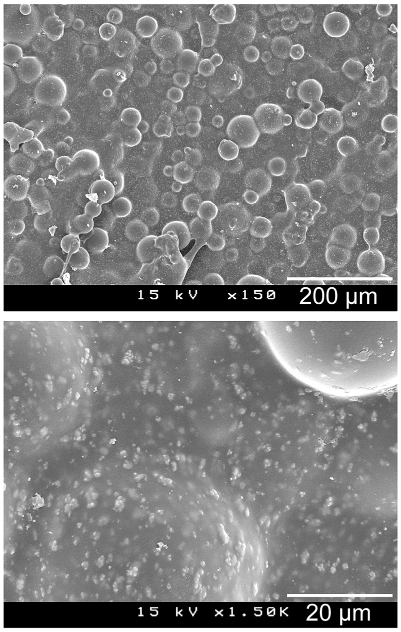

Figure 3-2: SEM micrograph of a control sample soaked for 21 days.

Through SEM micrographs, it is evident in Figure 3-3 that the shape of 13-93B3 particles used here are angular in nature and are covered with smaller chipped glass particles. The particle shapes are irregular due to the grinding methods used.

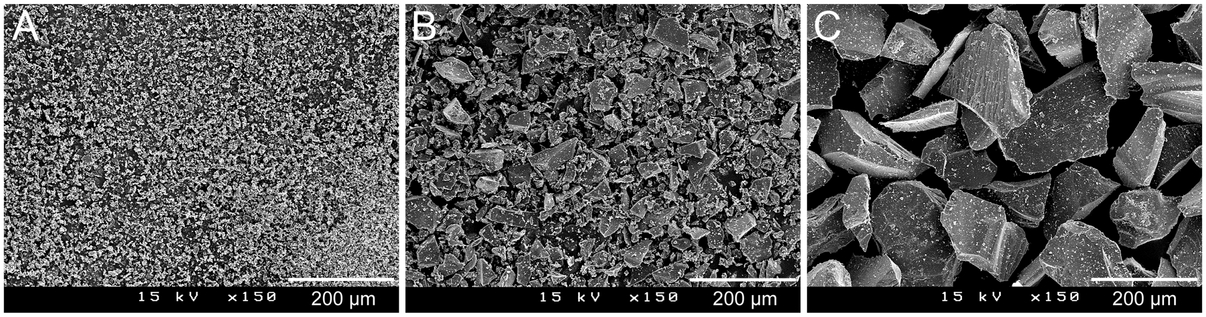

Figure 3-3: SEM micrographs of as-received 5 μm glass (A), 33 μm glass (B), and 100 μm glass (C).

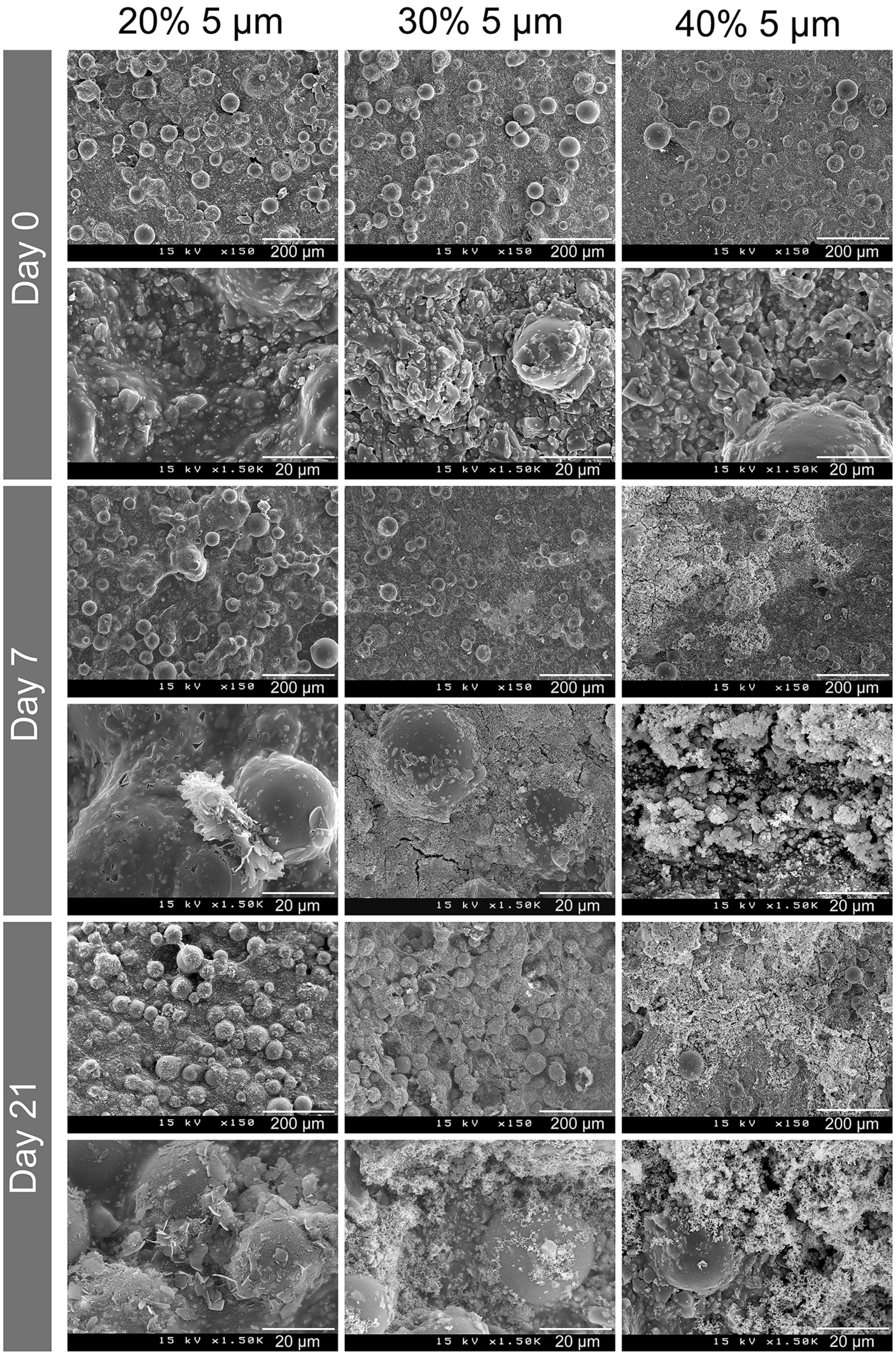

Figure 3-4: Surfaces of samples containing 5 μm glass after soaking for 0, 7, and 21 days.

5 µm Composites: The inclusion of 5 µm glass into the dry pellets are evidenced by the jagged bumps under the PMMA layer in Figure 3-4, which increase in frequency as the concentration of glass increases.

For 20% 5 µm, precipitates could be seen by Day 7, but surface coverage was sparse. Isolated areas showed small crystalline formations. By Day 21, the surface was covered with precipitate, and crystalline formations mixed with powdery precipitates could be seen.

For 30% 5 µm, a crystalline morphology could be seen on the surface by Day 7, as well as a thin layer of precipitate. Some larger precipitate structures had formed, as seen in Figure 3-5. By Day 21, the surface was more completely and thickly covered with larger precipitate particle sizes, and some craggy accumulations of precipitate were present.

For 40% 5 µm, at Day 7 the surface already had rounded structures and was partially carpeted with granular particles, and by Day 21 the surface was more thickly carpeted.

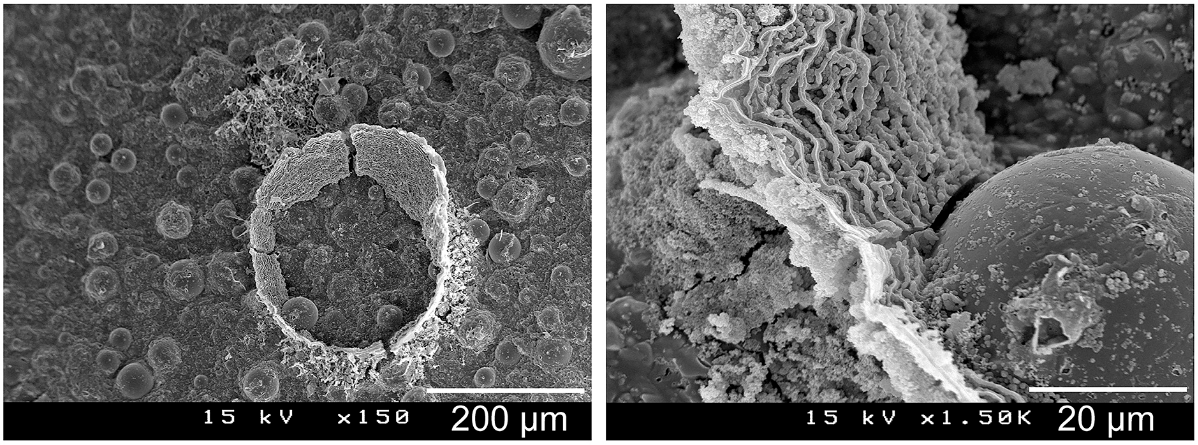

Figure 3-5: Left: Precipitate ring on a 30% 5 µm composite after 7 days of soaking. Right: Close-up of the structure.

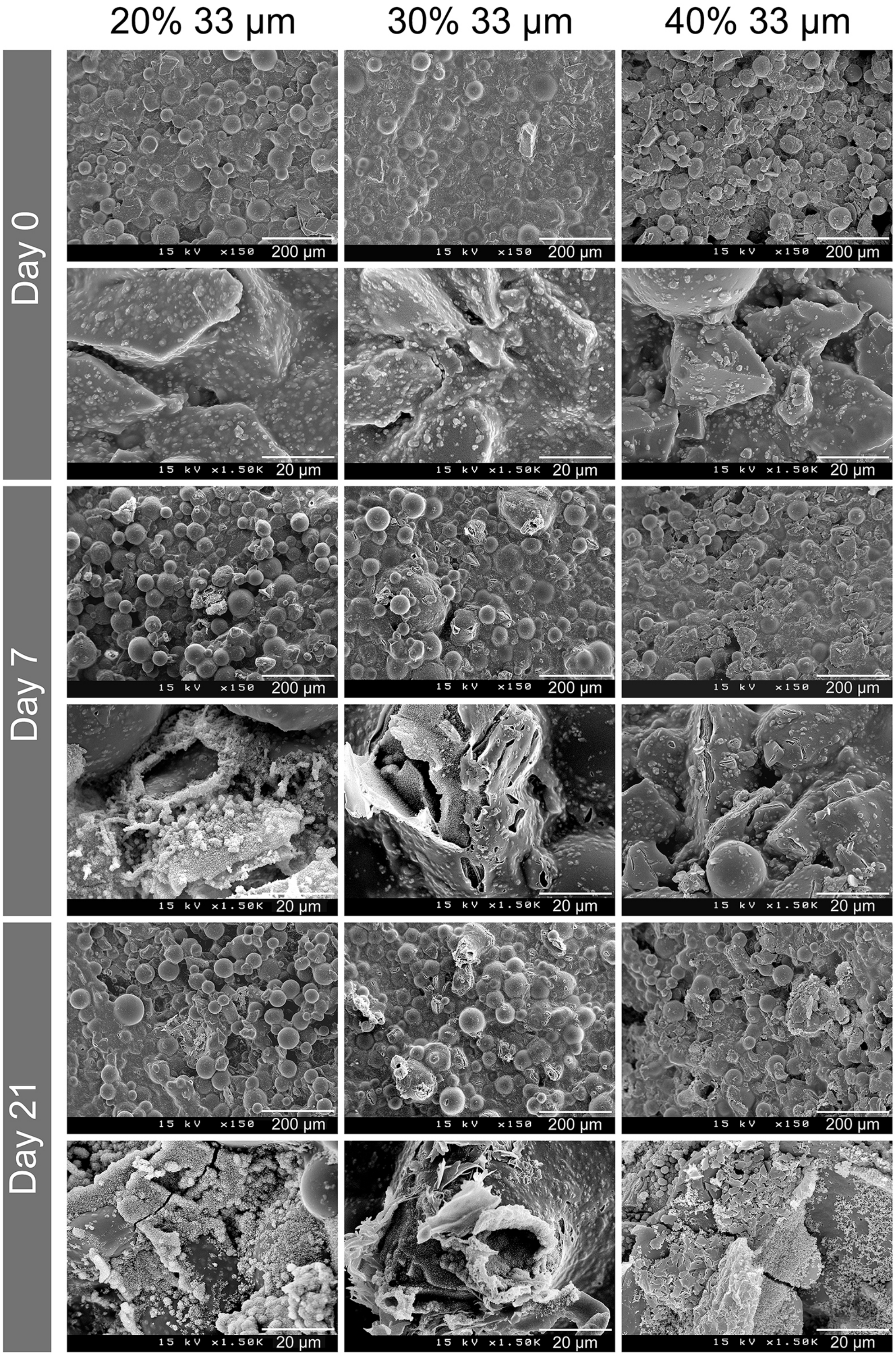

Figure 3-6: Surfaces of samples containing 33 µm glass after soaking for 0, 7, and 21 days.

33 µm Composites: In Figure 3-6, glass is evidently embedded in the bone cement and covered with a layer of PMMA in dry samples. For 20% 33 µm, after 7 days of soaking, precipitate has accumulated on sporadic areas on the surface, and some large structures are present. By Day 21, precipitate with a granular morphology had extended to cover more surface area as well as a strand-like form seen in Figure 3-7. Crystalline platelet forms that existed on the analogous 20% 5 µm pellets could not be seen.

For 30% 33 µm, some calcium phosphate growths have formed by Day 7, but they are restricted to areas surrounding surface glass, where clumps of precipitate crystals have formed, including spheres and elongated strands. By Day 21, the clumped precipitates have spread out further onto the cement surface.

For 40% 33 µm, by Day 7, large rounded precipitate structures had formed around surface pores, and the PMMA top layer was cleaved around the edges of embedded glass particles. By Day 21, the precipitate extended away from individual glass particles embedded in the matrix, and large precipitate structures had formed. The area surrounding these structures were carpeted with precipitate, including platelets and small spheres.

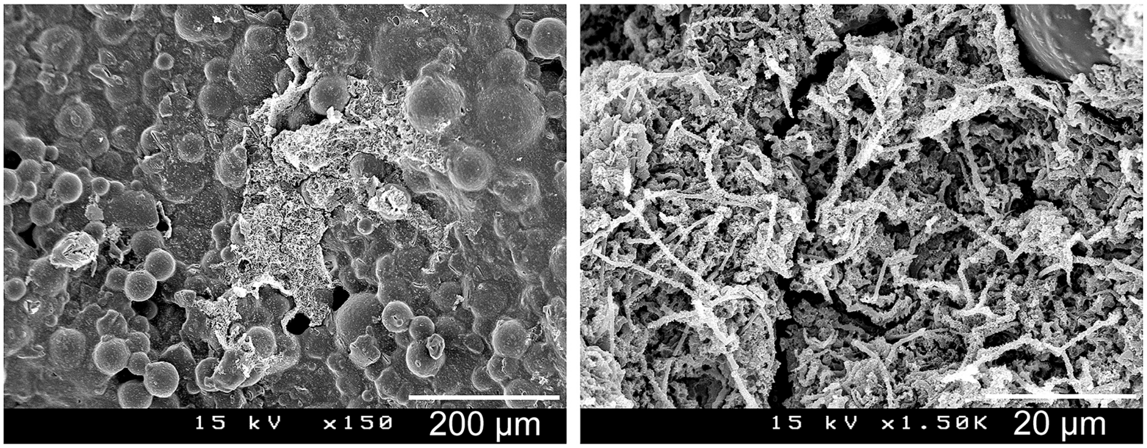

Figure 3-7: Left: Precipitate accumulation on 20% 33 µm after 21 days of soaking. Right: Close-up of the same structure.

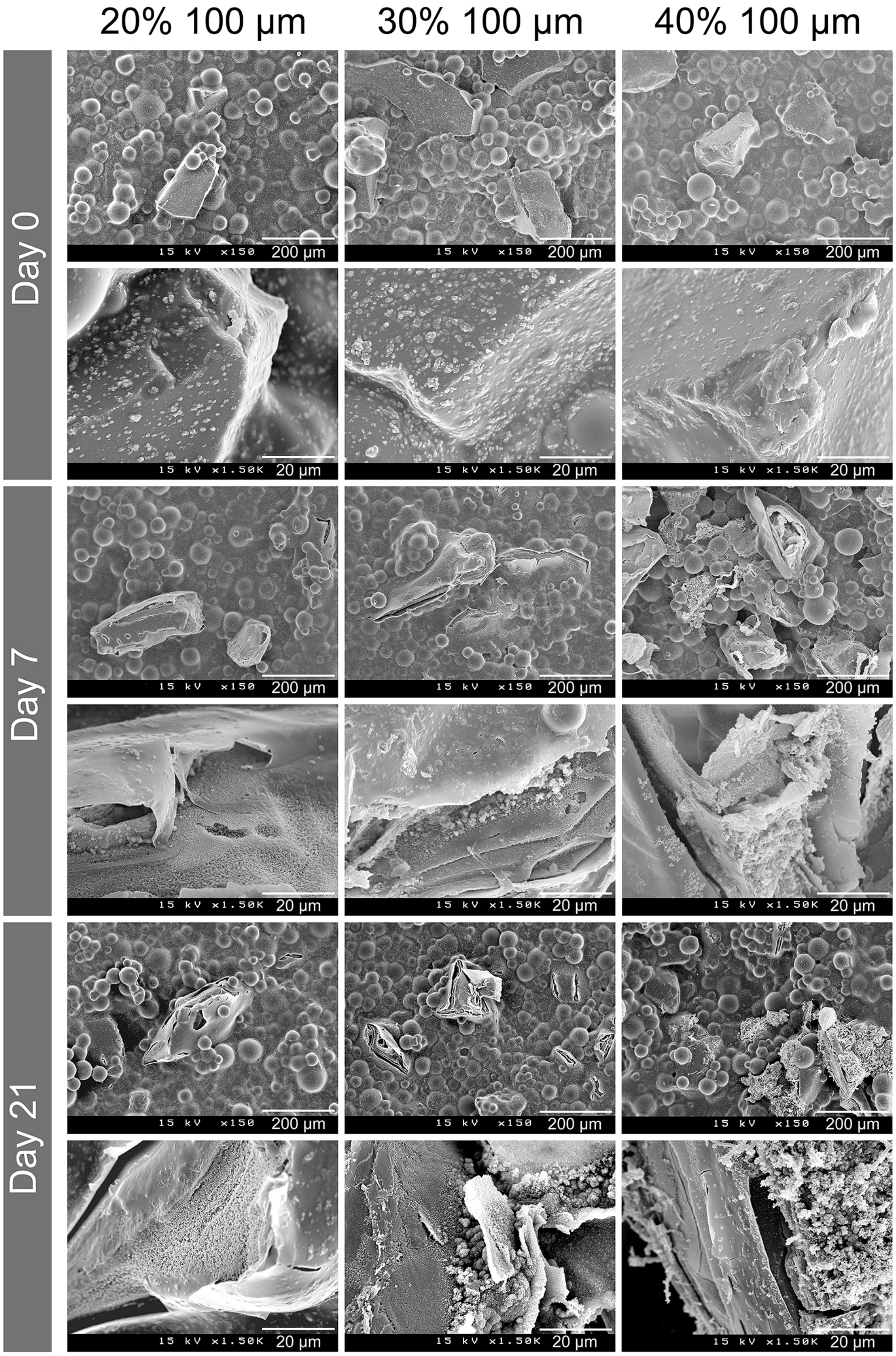

Figure 3-8: Surfaces of samples containing 100 µm glass after soaking for 0, 7, and 21 days.

100 µm Composites: Glass was consolidated into large particles, as seen in Figure 3-8, and for 20% 100 µm, the particles were sparsely distributed on the surface. When the samples were formed, the glass near the surface was covered with polymerized PMMA. After 7 days, the bone cement layers surrounding the glass particles in 20% 100 µm had torn, which directly exposed the glass to the solution. The surface of the glass had become textured, with small clumps of material clinging along edges. Degradation and precipitation appeared to be concentrated upon glass particles, with little precipitation away from the glass.

For 30% 100 µm, precipitation beyond the exposed glass was still sparse. By Day 7, the glass particles were showing signs of cleaving. By Day 21, the glass showed further signs of cleavage and degradation. The rounded clumps of precipitate on the glass were more prevalent and numerous in 30% 100 µm than in 20% 100 µm.

For 40% 100 µm, by Day 7, precipitate accumulation extended beyond the areas of exposed glass particles, and glass cleavage was more pronounced than in other formulations with 100 µm glass after the same amount of soaking time. Thin needles and platelets were evident. By Day 21, granular precipitate with strand-like protrusions surrounded the degraded glass and covered nearby surfaces. Large precipitate structures were also present.

For pellets containing glass particle sizes of 5 µm or 33 µm, rounded and concave accumulations of precipitate also formed upon the surface, as seen in Figures 3-5 and 3-9. The structures tended to be situated above a surface pore, and the PMMA-covered surface of the pellet could be seen at the bottom of the concave structures.

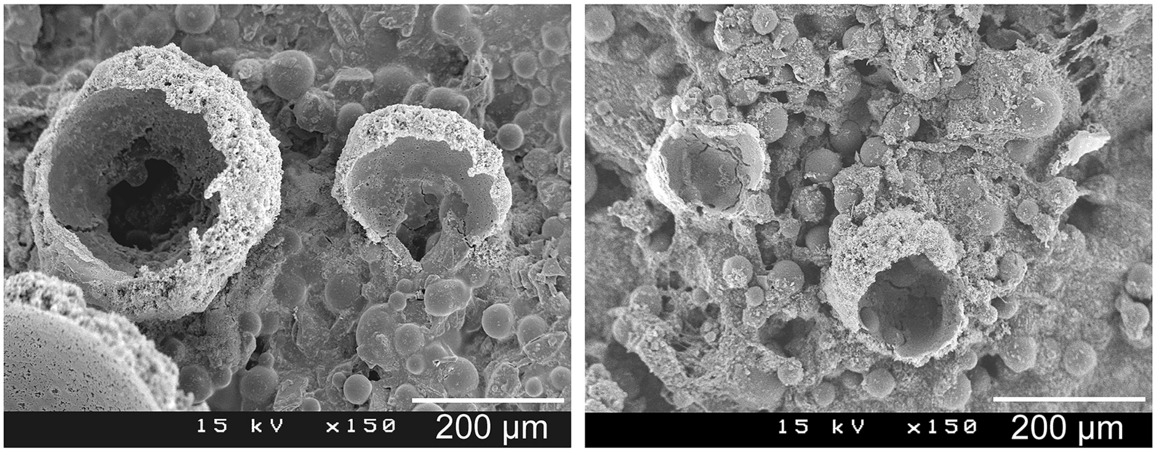

Figure 3-9: Left: Precipitate structures on 40% 33 µm after 7 days of soaking. Right: Precipitate structures on 30% 5 µm after 21 days of soaking.

3.4.2. Energy Dispersive X-ray Spectroscopy

3.4.2.1. Elemental Ratios

The values found for calcium, magnesium, and phosphorus concentrations are shown in Table 3-1. While the Ca/P ratios were lower than the 1.67 Ca/P ratio seen in stoichiometric hydroxyapatite, (Ca+Mg)/P ratios for 20% 5 µm and 40% 5 µm pellets soaked for 21 days approached 1.67.

The related EDS spectra are shown in Figure 3-10. The differences between 40% 5 µm and 20% 5 µm are not notable. The Cl peaks are attributable to the chlorine present in the PBS (Table 2-1), and the Al and Si peaks are negligible and likely from the environment.

Sample	Ca (mol%)	P (mol%)	Mg (mol%)	Ca:P	(Ca+Mg):P	Ca:Mg
20% 5 µm	7.81 ± 0.26	6.21 ± 0.29	2.77 ± 0.19	1.26	1.70	2.82
40% 5 µm	8.95 ± 0.51	7.02 ± 0.38	3.42 ± 0.3	1.27	1.76	2.62

Table 3-1: Table of elemental percentages and ratios of Ca, P, and Mg in samples soaked for 21 days.

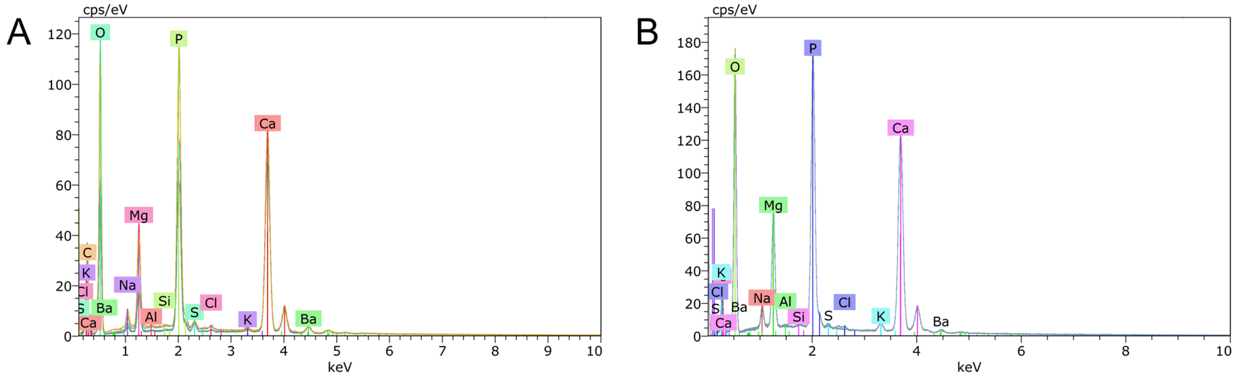

Figure 3-10: Representative EDS spectra for a 20% 5 µm sample soaked for 21 days (A) and a 40% 5 µm sample soaked for 21 days (B).

3.4.2.2. Elemental Mapping

Through elemental mapping seen in Figure 3-11, the precipitate upon a 20% 5 µm pellet soaked for 21 days was found to have an increased amount of calcium, phosphorus, and magnesium and lack carbon, sulfur, and barium relative to the surrounding surface. Oxygen was also concentrated in the precipitate.

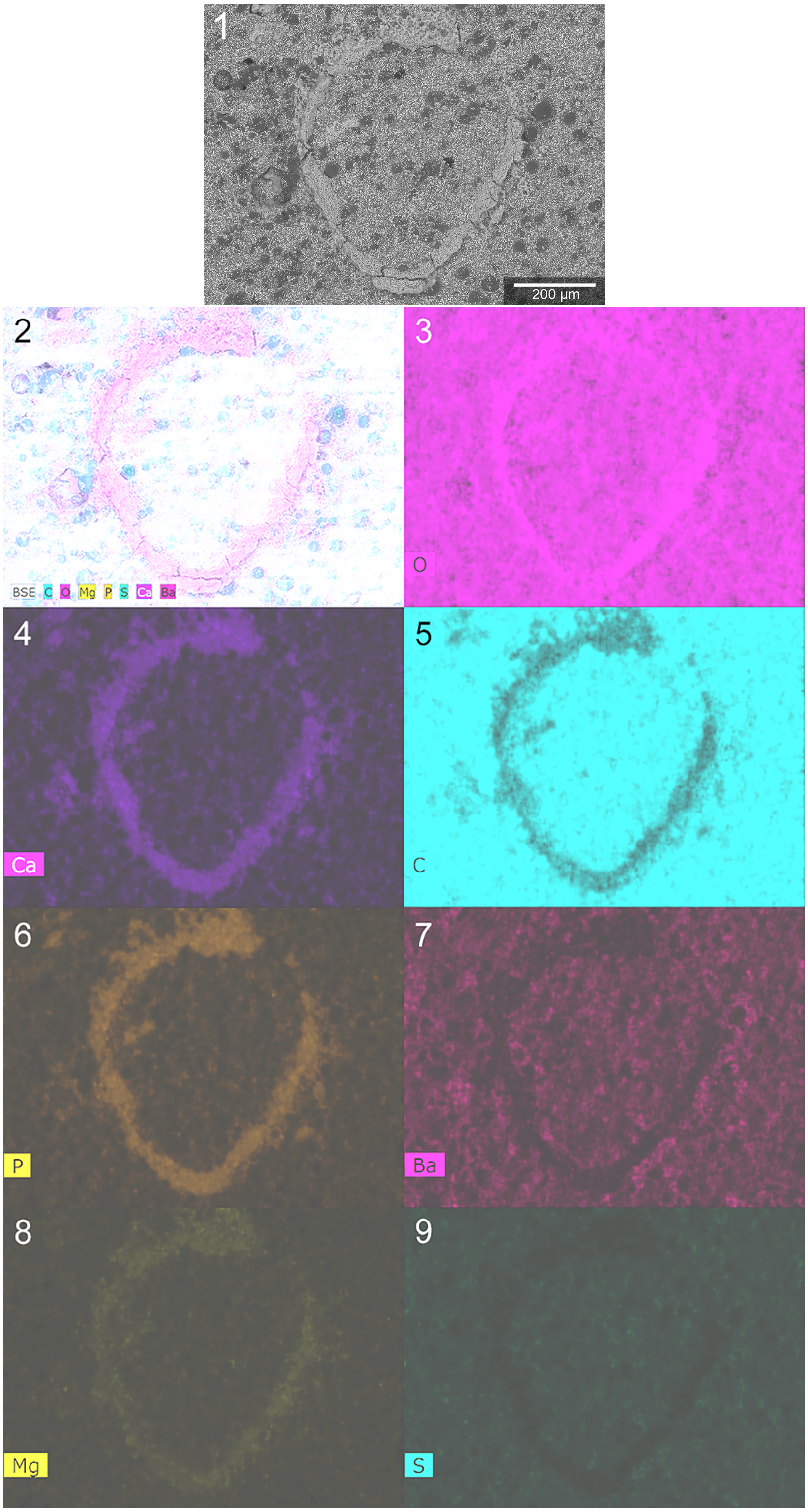

Figure 3-11: The original SEM micrograph of a ring of precipitate (1) and a corresponding EDS elemental analysis map of all elements studied combined (2), oxygen (3), calcium (4), carbon (5), phosphorus (6), barium (7), magnesium (1), and sulfur (9). The micrographs are from a 20% 5 µm pellet soaked for 21 days. Dark regions in (1) is thermal damage from the SEM technique used. All maps were evenly brightened in Adobe Photoshop CC 2017 to better illustrate the colors.

3.4.3. Fourier Transform Infrared Spectroscopy – Attenuated Total Reflection

Graphs comparing the FTIR data of the control and unconverted 13-93B3 glass with glass-containing samples are shown in Figure 3-12, and the peak assignments are detailed in Table 3-2. The control shown was soaked for 21 days; an unsoaked control (not shown) provided a spectrum nearly indistinguishable from the soaked control. The strongest peak, at 1726 cm^{-1}, was from the C=O stretch in the ester group in PMMA.[105]

The glass powder showed broad peaks at 1360 cm^{-1} and 715 cm^{-1}, which were indicative of B-O stretching and bending in BO_3 groups respectively, and a peak at 950 cm^{-1} showed B-O stretching in BO_4 units.[87,106]

The FTIR spectrum recorded from the dry 5 µm 20% sample had weaker versions of the control's peaks. The dry 30% and 40% 5 µm spectra had even weaker peaks. A peak from 950-1100 cm^{-1} centered at approximately 1030 cm^{-1} was noted after 21 days in all 5 µm samples, and this peak was attributed to PO_4^{3-}. The 560 cm^{-1} peak was less evident in 33 µm samples and appeared as a shoulder instead, which became more prominent as soak time increased and as glass concentration increased. The ν_4 PO_4^{3-} peak at 603 cm^{-1} was overlapped by the SO_4^{2-} peak at 608 cm^{-1} and was therefore difficult to see. Signs of CO_3^{2-} peaks were not detected at 870-879 cm^{-1}, 1414 cm^{-1}, 1455 cm^{-1}, or 1545 cm^{-1}, but, if present, may have been hidden by peaks caused by the bone cement's components.[107] For 5 µm samples, a broad band at 3000-3500 cm^{-1} increased in intensity as the loading amount and soak time increased. For 100 µm-loaded samples, no notable changes were seen throughout the soak periods and glass concentration. The OH stretch at 3569 cm^{-1}, typical of hydroxyapatite, was not observed in any samples.[108]

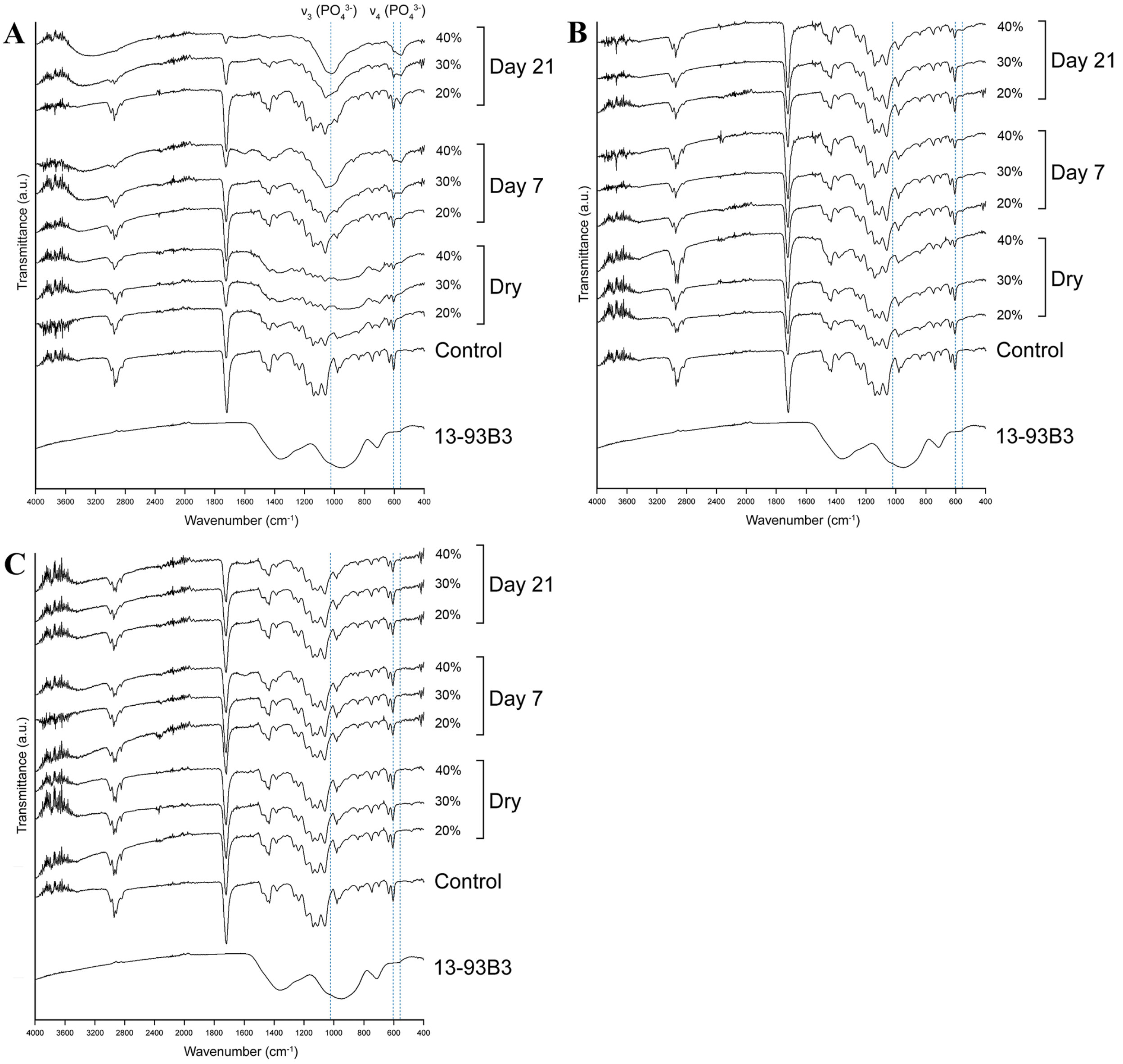

Figure 3-12: Representative FTIR-ATR spectra of samples containing 5 µm glass (A), 33 µm glass (B), and 100 µm glass (C). Samples soaked for 0 days are termed here as "dry". The spectra for a control sample soaked for 21 days and for as-received 5 µm glass are presented here for comparison. Dotted lines designate peaks of interest explained in the text.

Peak (cm^{-1})		Assignment	Reference
480	w	out-of-plane deformation of ester (ν_6)	105
556	m	PO_4^{3-} bending (ν_4)	87
603	m	PO_4^{3-} bending (ν_4)	87
608	m	SO_4^{2-} out-of-plane bending	109
636	m	SO_4^{2-} out-of-plane bending	109
704	w	out-of-plane bending in phenyl group in styrene	110
715	m b	B-O bending in BO_3	106
748	m	antisymmetric stretching of C-C skeletal mode	105
840	w	CH_2 rocking	105
912	w	CH_3 rocking	111
950	s b	B-O stretching in BO_4	106
964	m	α-CH_3 rocking	105
984	m	O-CH_3 rocking	105
1030	s	PO_4^{3-} antisymmetric stretching (ν_3)	87
1060	s	antisymmetric stretching of C-C skeletal mode	105
1112	s	antisymmetric stretching of C-C skeletal mode	105
1144	s	C-O-C antisymmetric stretching	105
1188	s	C-O-C antisymmetric stretching	105
1236	m	C-O stretching	105
1268	m	C-O stretching	105
1360	s	B-O stretching in BO_3	106
1385	w	symmetric bending of C-H in α-CH_3	105
1433	m sh	symmetric bending of C-H in O-CH_3	105
1446	m	symmetric bending of C-H in alpha CH_3	105
1480	m	CH_2 bending	105
1724	s sh	C=O stretching	105
2848	m	combination band involving O-CH_3	105
2920	s	combination band involving O-CH_3; symmetric stretching of CH_2	105
2948	s	symmetric stretching of C-H in α-CH_3 and in O-CH_3; antisymmetric stretching of CH_2	105
2992	m	antisymmetric stretching of C-H in α-CH_3 and O-CH_3	105
3000-3500	m b	absorbed H_2O	112

Table 3-2: Peak assignments for the FTIR-ATR spectra shown in Figure 3-12. For peak characteristics, w = weak, m = medium, s = strong, sh = sharp, b=broad. The highlighted peak assignments are the identifying peaks used for hydroxyapatite.

3.4.4. Micro-Raman Spectroscopy

Raman spectra are shown in Figure 3-13 along with peak assignments in Table 3-3. The unsoaked control's peaks correlated with literature values for PMMA, styrene, and barium sulfate. Immersing the control in PBS appeared to cause changes to the peaks. Peaks at ~670 and ~760 cm^{-1} were introduced after a week of soaking and were considered to be recording artifacts. These artifacts near 500 cm^{-1} shielded the C-C-O peak at 486 cm^{-1} from view.

The glass mixtures presented peaks that are seen from the soaked control, but the peaks at 602, 812, 972, 987, 1004, and 1457 cm^{-1} from the bone cement have been decreased. The sharpness of the ν_1 PO_4^{3-} peak at 964 cm^{-1} appeared to decrease relative to other peaks from 7 days to 21 days for 100 µm samples, and this was more evident in 40% 100 µm.

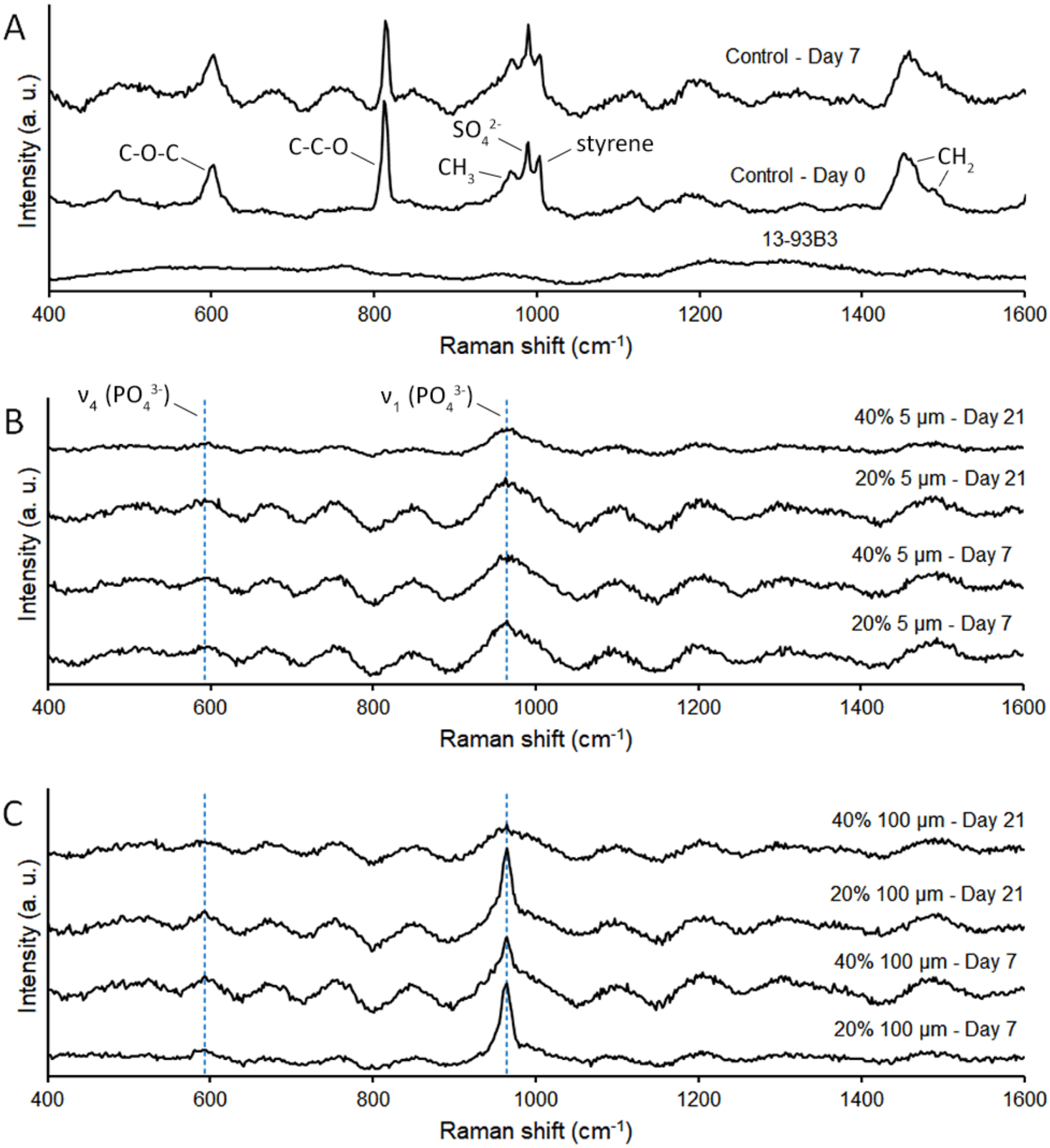

Figure 3-13: Raman spectra obtained from various surfaces: a control soaked for 0 days, a control soaked for 7 days, and as-received 100 µm glass (A); 20% 5 µm and 40% 5 µm after 7 and 21 days of soaking (B); and 20% 100 µm and 40% 100 µm after 7 and 21 days of soaking (C). Dotted lines designate peaks of interest explained in the text.

Peak (cm^{-1})		Assignment	Reference
486	w	C-C-O out-of-plane deformation	[105]
594	w	PO_4^{3-} bending (ν_4)	[113]
602	s	C-C-O symmetric stretch (ν_1)	[114]
616	m	SO_4^{2-} out-of-plane bending	[115]
812	s sh	C-O-C symmetric stretch	[114]
849	w	CH_2 rocking	[105]
964	s	PO_4^{3-} symmetric stretching (ν_1)	[113]
972	m sh	α-CH_3 rocking	[105]
987	s sh	SO_4^{2-} symmetric stretch	[115]
1004	m sh	aromatic breathing mode of styrene	[116]
1033	w	C-H bending in aromatic ring of styrene	[116]
1110	w	skeletal C-C antisymmetric stretch	[105]
1128	w	C-O-C antisymmetric stretch	[105]
1190	w	C-O-C antisymmetric stretch	[105]
1204	w	C-C stretch in styrene	[117]
1238	w	C-O stretch	[105]
1330	w	CH_2 wagging	[117]
1393	w	symmetric bending of C-H in α-CH_3	[105]
1457	s	CH_2 bending	[117]
1489	m	CH_2 bending	[105]

Table 3-3: Peak assignments for the Raman spectra shown in Figure 3-13. For peak characteristics, w = weak, m = medium, s = strong, sh = sharp. The highlighted peak assignments are the identifying peaks used for hydroxyapatite.

3.5. Discussion

Overall, the thin layer of PMMA that covered surface glass particles formed cracks as the samples soaked. This may have been due to pressure exerted onto the PMMA layer by the dissolving glass. The coatings of precipitate that formed on the surfaces were typically sporadic and uneven, and this was likely due to the heterogeneity of the cement causing differing local concentrations of glass. The morphology of the precipitate was also affected by the size and concentration of glass added. Having more glass in the composite and in a smaller particle size appeared to allow the glass to dissolve faster and more completely, forming more widespread precipitation. On bone cement containing 100 µm glass, more crystallized hydroxyapatite formed on the surfaces of exposed glass particles.

Solution pH appeared to affect the morphologies of the precipitate. In literature, hydroxyapatite formed in sheets at a solution pH of 7.5, and at a high pH such as 10, amorphous calcium phosphate first formed rapidly around nucleation sites before crystallizing into hydroxyapatite, creating small particles.[118] In Figure 3-4, 20% 5 µm samples have platelet-like crystalline precipitates, while the higher-loaded samples had more granular precipitate formations. From Figure 2-5a, for 5 µm samples, the 20% loading also had the most moderate pH values, culminating in an average pH of 8.63 after 21 days of soaking, while the 30% loading had a solution pH of 8.88 and the 40% loading had a solution pH of 9.13 by that time. Figures 3-5 and 3-7 also show oriented precipitates that formed in environments with a finishing pH of 8.79 and 8.47, respectively. For 100 µm samples, which maintained low pH values relative to other groups, the morphology was more orderly than in 5 µm samples, and this is reflected in the strong ν_1 PO_4^{3-} peaks seen in Figure 3-13c. Hydroxyapatite in the shape of plates, like those seen on 20% 5 µm samples at a relatively lower pH value, has been found in organic sources, such as bone.[119] In the body, the fluid environment would be continuously flushed by the body, and so the precipitate morphologies seen at higher pH conditions may not form *in vivo*.[120]

Bowl- and ring-shaped structures of precipitate, such as those seen in Figures 3-5, 3-9, and 3-11, may have formed around air bubbles that exited the samples after immersion and remained on the sample surfaces, providing a nucleation site. Such structures were interspersed on samples, and they likely formed in areas with greater-than-average amounts of glass to be able to accumulate enough material to create these structures. The surfaces immediately surrounding the structures were also covered with precipitate. The texture of this surrounding precipitate, as seen in the close-up in Figure 3-5, is small and rounded, and this texture has been seen in hydroxyapatite deposits before.[58,69] As with high pH values, these formations may not occur in *in vivo* versions of this study due to the dynamic environment within the body.

The (Ca+Mg)/P ratios of the precipitates studied were close to 1.67, which would be expected for a magnesium-substituted hydroxyapatite arising from glasses doped with Mg.[66] However, the Ca/Mg ratios in the precipitates studied were high and the Ca/P ratios were low compared to values reported for precipitate on soaked 13-93B3 fibers.[69] The magnesium may have become saturated in the solution used here, causing the excess to enter the precipitate and increase the Ca/Mg ratio. Bertinetti et al. had hypothesized about the formation of a thin layer of a magnesium-hydrated phase on apatite surfaces when in solutions of high magnesium content.[121] Due to the low Ca/P ratios, the precipitate in the areas studied may have also still been in the process of transforming into hydroxyapatite, as magnesium ions slow down conversion.[122] On the elemental mapping, the calcium, oxygen, phosphorus, and magnesium amounts are higher on the precipitate than on the rest of the surface. This suggests that the precipitate is made of a magnesium incorporated apatite, as would be predicted for a product of 13-93B3.[69] The precipitate contained less barium, sulfur, and carbon than the surrounding areas, which would be expected because the presence of these elements would represent areas of bone cement not covered by precipitate. Barium sulfate present in the bone cement formulation is composed of barium and sulfur, and carbon is a component of PMMA.

From the FTIR-ATR data, representative spectra of the control showed peaks that correlated well with reported values for PMMA and barium sulfate. The broad quality of the ν_3 PO_4^{3-} peak at 1030 cm^{-1} for 5 µm samples after 21 days of soaking indicated poorly crystallized hydroxyapatite, which would be expected due to the incorporation of magnesium.[69,112,123] From the same readings, the asymmetric bending frequency (ν_4) of phosphate at 600 cm^{-1} split into a doublet at 556 cm^{-1} and 603 cm^{-1}, which also indicated hydroxyapatite. As the glass concentration increased, the peaks became less distinct from each other. More separation between the peaks meant higher crystallization.[124] Therefore, after 21 days of soaking the 20% 5 µm sample appeared to have the most crystallized hydroxyapatite, with 30% 5 µm samples showing less crystallization and 40% 5 µm samples having even lower crystallization. The 5 µm glass findings were validated by the SEM results, which showed that platelets had formed on the 20% 5 µm surface instead of the scattered powders seen in samples containing higher concentrations of 5 µm glass. The broad band also seen at 3000-3500 cm^{-1} in 5 µm samples was attributed to water, which would have been absorbed by the precipitate.[112] This band would not be seen in samples with a surface area mainly composed of hydrophobic PMMA.

FTIR-ATR spectra were collected from the smooth surfaces of the samples, and these surfaces formed when the samples were curing in PTFE molds. When the cement was packed against the sides of the mold, the polymerizing matrix filled in the space around fillers. Smooth sample surfaces did not have the beaded texture seen in the SEM micrographs taken, and so styrene peaks at 1493 cm^{-1} and 1603 cm^{-1} from C=C aromatic stretches and at 3026 cm^{-1} from C-H aromatic stretches were not detected.[125] This smoothness limited the surface area on the composites covered by larger glass particles (33-100 µm) and their precipitates, which in turn limited their expression on FTIR-ATR readings.

In the Raman spectra, samples of 100 µm may have had a sharper peak at 964 cm^{-1} because of the moderate pH and because the surface of the large glass particles would constantly interact with dissolving material from within the glass, causing more complete crystallization. The 100 µm samples also had a small peak near 594 cm^{-1} indicative of ν_4 PO_4^{3-}, just as seen in

FTIR data. The position of the ν_1 PO_4^{3-} peak is critical to differentiate the precipitate between various forms of calcium phosphate, and at 964 cm^{-1} as seen in Figure 3-13, this indicates hydroxyapatite. Shifts in this peak's position would represent other forms. For example, a broad peak centered at 950 cm^{-1} would indicate amorphous calcium phosphate, with its broad quality resulting from the lack of crystallinity.[126] If β-tricalcium phosphate was a prevalent form, peaks at 946-949 cm^{-1} and 971 cm^{-1} would be seen instead.[127]

A substitution of calcium with magnesium in hydroxyapatite would cause changes to the bond lengths and the matrix structure of the material, as magnesium is a smaller ion.[128,129] This partial substitution increases the disorder of the crystallinity of the hydroxyapatite, lowering the intensity of PO_4^{3-} spectra and increasing the peak width.[130] Because the 964 cm^{-1} peak broadens as the amount of magnesium rises, it is possible that the precipitate on the samples incorporated more magnesium over time, as seen in 40% 100 µm, and that 5 µm samples incorporated more magnesium than 100 µm samples did. A lack of crystallinity may also come from the small size of the precipitate particles, which were seen with SEM. Raman spectra did not differ noticeably between samples containing 5 µm glass soaked for 7 days and 21 days.

The ν_1 PO_4^{3-} peak at 964 cm^{-1} was the most reliable indicator of a phosphate-based precipitate in the Raman spectra; other related phosphate peaks were not visible, aside from weak ν_1 PO_4^{3-} peaks in 100 µm samples at 594 cm^{-1}. Other peaks that could have been present, such as ν_2 or ν_3 PO_4^{3-}, were not visibly identified and may have been shielded by the peaks seen in the Day 7 control. The broad peak near 960 cm^{-1} in all composite spectra was not considered to be conclusive for amorphous calcium phosphate because the peak was not centered around 950 cm^{-1} and had appeared to be present in the spectra of the Day 7 control. However, it is noted that magnesium ions in the precipitate can help stabilize amorphous calcium phosphate and slow down its conversion process to hydroxyapatite.[122]

Micro-Raman peaks differed from FTIR-ATR peaks because some molecular vibrations are more Raman-active than IR-active and vice versa.[103] The Raman spectra were also directly sampled from spots on exposed glass, which differed from the FTIR-ATR technique of scanning a large and smooth surface area. FTIR-ATR could detect precipitate bonds as long as the precipitate covered enough surface area to overcome the bone cement spectra, but the micro-Raman technique collected spectra from small, isolated areas of precipitate.

While the incorporation of magnesium into hydroxyapatite lowers its crystallinity, this ionic addition would be beneficial for bone growth and attachment around the material. Biological hydroxyapatite contains ionic substitutions for calcium, which means that the magnesium-substituted hydroxyapatite identified in this study would better mimic natural apatite than would stoichiometric hydroxyapatite.[131] Human bone already contains 0.47 wt.% of magnesium, and this similarity to natural bone material could boost its osteoconductivity.[66,70] Magnesium encourages osteoblast formation for bone building, which would help regrow bone lost during a joint replacement surgery.[65] The presence of magnesium has been shown to improve the attachment of living bone onto surfaces, which would help further attach the composites studied here to surrounding bone and reduce the surface area on the cement that living tissue (and therefore the immune response) cannot reach.[68]

3.6. Conclusion

The precipitate that accumulated on the composites was concluded to be a hydroxyapatite-like mineral that included substitutions of magnesium ions in place of calcium. Magnesium incorporated in the precipitate layer on the surface of the cement could increase the success of bone growth around the cement. This would help better attach the bone cement and connected implants onto the native bone, recoup bone removed during surgery, and reduce the surface area on the bone cement that is open to biofilm formation.

One limitation of this study was the sample size used for SEM-EDS readings. The EDS elemental map in Figure 3-11 is from mapping one sample, and in the future, EDS mapping could be expanded to track the progression of elemental distributions over time spent soaking for more groups to compare them. The groups studied in the EDS and micro-Raman tests could be expanded as well to include data from 33 µm groups and for soak lengths besides 7 and 21 days. This would give further insight into the precipitate formation process and show if any other phases of calcium phosphate had formed during the soaking interval. The various morphologies seen under SEM may also have different ratios of Mg, Ca, and P, which could be studied by collecting further EDS data from these groups.

A weakness of the FTIR-ATR technique used here is that the spectra become noisy at wavelengths less than 650 cm^{-1}, so data at higher wavelengths should be considered to be more reliable. Another limitation of this technique is that a smooth surface on the samples was used to collect FTIR spectra due to its increased ability to interface with the crystal surface, which misses information about the rough sides of the samples and their rounded sides.

Analyzing pure PBS with micro-Raman spectroscopy may help locate the source of the unidentifiable peaks that appeared in soaked samples in Figure 3-13. The resolution of the micro-

Raman data could also have been improved by using a more powerful magnification, such as 100x, and by collecting the data for longer than five seconds at a time.

X-ray diffraction (XRD) could be utilized as an added measure of the crystallization of the precipitates. Studying the angles of diffraction caused by the precipitate would further confirm the identity of the species forming on the sample surfaces over time. This would be another way to discern between various forms of calcium phosphate and hydroxyapatite and their crystallinity. Due to the poorly crystallized forms of hydroxyapatite seen on composites with higher loading amounts, this technique would be most effective for composites with a 20% glass loading.

Some samples, such as the 40% 33 μm pellet in Figure 3-1, were markedly more porous on their rounded sides than the controls were. Further studies can measure the porosity of these samples and take SEM images of surface locations not studied here. Samples can also be cut width-wise to examine their cross sections and see how far inwards the pores penetrate the samples. EDS and micro-Raman spectroscopy spectra from precipitate inside the of pores can be analyzed to see how precipitate in these locations may differ in composition from surface precipitate.

The extent of possible bone cell proliferation on the composites could be tested *in vitro* to make sure that the precipitate does in fact encourage bone growth more than the commercial bone cement control. If successful, then this test could be continued *in vivo* in a rat model as has been done before for a mixture of PMMA and silicate bioactive glass.[37]

Chapter 4: Thesis Conclusion and Future Directions

Borate bioactive glass particles of 13-93B3 can be mixed into SmartSet's dry powder component before polymerization to achieve noticeable changes in the properties of the cured product while not compromising the mechanical integrity of the cement. Changing the amount and particle size of 13-93B3 in the bone cement composite affected the bone cement's compressive strength, though this value did not fall below the ASTM and ISO minimum standards. The weight loss and water uptake were also found to increase with the addition of bioactive glass. However, this did not exceed 1.5% and 6%, respectively, which helped to preserve the mechanical strength of the composites. The pH and boron ionic concentration in solution increased in pH as the glass in the composites continued to dissolve and enter the solution, which was expected. After soaking, a white precipitate was visible on the surfaces of the composite samples, and this was especially evident and widespread on 5 µm samples. The precipitate became increasingly amorphous and granular as the glass loading increased. This was due to the incorporation of magnesium, which is an element that further encourages bone growth and therefore increases potential bone attachment to the cement.

Of the groups tested in this work, samples with a small glass particle size (5 µm) and a loading of 30-40% seemed to be the most effective at forming a precipitate layer incorporated with magnesium while maintaining the mechanical requirements of clinically-used bone cement. While these groups caused a high pH and boron concentration in the solution, this would be flushed away *in vivo* and not be a significant concern.

Because the borate bioactive glass in the composites showed signs of dissolving and forming precipitate while the composites remained above ASTM and ISO standards for compressive strength, it can be concluded that composites of bone cement and borate bioactive glass 13-93B3 could be used in applications for commercial bone cement while also providing material for bone ingrowth and potentially increasing antibiotic delivery. The most direct next step is to incorporate antibiotics, such as vancomycin and gentamicin, into the bioactive glass and bone cement composites. The elution rates of the antibiotic and its effectiveness at suppressing bacteria *in vitro* could then be studied. Since the addition of antibiotics may further affect the mechanical properties of the composites, the mechanical integrity of the composites would have to be monitored again. Testing osteoblast viability on the composite surfaces would also be helpful to ensure that the composites would not adversely affect bone growth.

Other commercial bone cements beyond SmartSet MV can also be tested for this application. Palacos R is another type of bone cement mentioned in Chapter 1 that has been studied for its ability to deliver antibiotics, for example. The incorporation of 13-93B3 and antibiotics into these bone cements may cause different mechanical changes and glass dissolution rates than those seen in this work.

References

1. Carr AJ, Robertsson O, Graves S, et al. Knee replacement. *The Lancet.* 2012;379(9823):1331-1340.
2. Wroblewski BM, Siney PD, Fleming PA. Charnley low-frictional torque arthroplasty in patients under the age of 51 years. *The Journal of Bone and Joint Surgery.* 2002;84-B(4):540-543.
3. Bozic KJ, Kurtz SM, Lau E, et al. The Epidemiology of Revision Total Knee Arthroplasty in the United States. *Clinical Orthopaedics and Related Research®.* 2010;468(1):45-51.
4. Kurtz SM, Lau E, Schmier J, Ong KL, Zhao K, Parvizi J. Infection Burden for Hip and Knee Arthroplasty in the United States. *The Journal of Arthroplasty.* 2008;23(7):984-991.
5. Tande AJ, Patel R. Prosthetic joint infection. *Clin Microbiol Rev.* 2014;27(2):302-345.
6. Del Pozo JL, Patel R. Clinical practice. Infection associated with prosthetic joints. *N Engl J Med.* 2009;361(8):787-794.
7. Parvizi J, Zmistowski B, Berbari EF, et al. New Definition for Periprosthetic Joint Infection: From the Workgroup of the Musculoskeletal Infection Society. *Clinical Orthopaedics and Related Research®.* 2011;469(11):2992.
8. Chen AF, Della Valle CJ, Rao N, Parvizi J. Treatment of the Infected Total Knee. *Operative Techniques in Orthopaedics.* 2012;22(4):236-246.
9. Kalore NV, Gioe TJ, Singh JA. Diagnosis and Management of Infected Total Knee Arthroplasty. *The Open Orthopaedics Journal.* 2011;5:86-91.
10. Lombardi AV, Jr., Karnes JM, Berend KR. A motion maintaining antibiotic delivery system. *J Arthroplasty.* 2007;22(4 Suppl 1):50-55.
11. Bengtson S, Knutson K. The infected knee arthroplasty: A 6-year follow-up of 357 cases. *Acta Orthopaedica Scandinavica.* 1991;62(4):301-311.
12. Trampuz A, Zimmerli W. Diagnosis and treatment of implant-associated septic arthritis and osteomyelitis. *Current Infectious Disease Reports.* 2008;10(5):394-403.
13. Kurtz SM, Lau E, Watson H, Schmier JK, Parvizi J. Economic Burden of Periprosthetic Joint Infection in the United States. *The Journal of Arthroplasty.* 2012;27(8, Supplement):61-65.e61.
14. Kurtz S, Ong K, Lau E, Mowat F, Halpern M. Projections of primary and revision hip and knee arthroplasty in the United States from 2005 to 2030. *J Bone Joint Surg Am.* 2007;89(4):780-785.
15. Kuehn KD, Ege W, Gopp U. Acrylic bone cements: composition and properties. *Orthop Clin North Am.* 2005;36(1):17-28, v.
16. Seyyed Hosseinzadeh HR, Emami M, Lahiji F, Sina A, Masoudi A, Emami S. The Acrylic Bone Cement in Arthroplasty. 2013.
17. Charnley J. Anchorage of the Femoral Head Prosthesis to the Shaft of the Femur. *J Bone Joint Surg.* 1960;43B:28-30.
18. Lopes P, Garcia MP, Fernandes MH, Fernandes MH. Properties and osteoblast cytocompatibility of self-curing acrylic cements modified by glass fillers. *J Biomater Appl.* 2013;28(4):498-513.

19. Lewis G. Alternative acrylic bone cement formulations for cemented arthroplasties: present status, key issues, and future prospects. *J Biomed Mater Res B Appl Biomater.* 2008;84(2):301-319.
20. Spierings PTJ. Testing and Performance of Bone Cements. In: *The Well-Cemented Total Hip Arthroplasty: Theory and Practice.* Berlin, Heidelberg: Springer Berlin Heidelberg; 2005:67-78.
21. Depuy Orthopaedics I. SmartsSet MV Bone Cement: Instruction Leaflet. 2009.
22. Kwon TY, Bagheri R, Kim YK, Kim KH, Burrow MF. Cure mechanisms in materials for use in esthetic dentistry. *J Investig Clin Dent.* 2012;3(1):3-16.
23. Sideridou ID, Achilias DS, Karava O. Reactivity of Benzoyl Peroxide/Amine System as an Initiator for the Free Radical Polymerization of Dental and Orthopaedic Dimethacrylate Monomers: Effect of the Amine and Monomer Chemical Structure. *Macromolecules.* 2006;39(6):2072-2080.
24. Nelson CL. The Current Status of Material Used for Depot Delivery of Drugs. *Clinical Orthopaedics and Related Research.* 2004;427:72-78.
25. Tunney M, Ramage G, Patrick S, Nixon J, Murphy P, Gorman S. Antimicrobial susceptibility of bacteria isolated from orthopedic implants following revision hip surgery. *Antimicrobial Agents and Chemotherapy.* 1998;11:3002-3005.
26. Squire MW, Ludwig BJ, Thompson JR, Jagodzinski J, Hall D, Andes D. Premixed antibiotic bone cement: an in vitro comparison of antimicrobial efficacy. *J Arthroplasty.* 2008;23(6 Suppl 1):110-114.
27. Jiranek WA, Hanssen AD, Greenwald AS. Antibiotic-Loaded Bone Cement for Infection Prophylaxis in Total Joint Replacement. *Journal of Bone & Joint Surgery.* 2006;88(11):2487-2500.
28. Moojen DJ, Hentenaar B, Charles Vogely H, Verbout AJ, Castelein RM, Dhert WJ. In vitro release of antibiotics from commercial PMMA beads and articulating hip spacers. *J Arthroplasty.* 2008;23(8):1152-1156.
29. Klekamp J, Dawson JM, Haas DW, DeBoer D, Christie M. The use of vancomycin and tobramycin in acrylic bone cement: Biomechanical effects and elution kinetics for use in joint arthroplasty. *The Journal of Arthroplasty.* 1999;14(3):339-346.
30. Neut D, van de Belt H, van Horn JR, van der Mei HC, Busscher HJ. The effect of mixing on gentamicin release from polymethylmethacrylate bone cements. *Acta Orthopaedica Scandinavica.* 2003;74(6):670-676.
31. van de Belt H, Neut D, Uges DRA, et al. Surface roughness, porosity and wettability of gentamicin-loaded bone cements and their antibiotic release. *Biomaterials.* 2000;21(19):1981-1987.
32. McConoughey SJ, Howlin RP, Wiseman J, Stoodley P, Calhoun JH. Comparing PMMA and calcium sulfate as carriers for the local delivery of antibiotics to infected surgical sites. *J Biomed Mater Res B Appl Biomater.* 2015;103(4):870-877.
33. Davies D. Understanding biofilm resistance to antibacterial agents. *Nat Rev Drug Discov.* 2003;2(2):114-122.
34. del Pozo JL, Patel R. The challenge of treating biofilm-associated bacterial infections. *Clin Pharmacol Ther.* 2007;82(2):204-209.
35. ter Boo G-JA, Grijpma DW, Moriarty TF, Richards RG, Eglin D. Antimicrobial delivery systems for local infection prophylaxis in orthopedic- and trauma surgery. *Biomaterials.* 2015;52:113-125.

36. Heikkilä JT, Aho AJ, Kangasniemi I, Yli-Urpo A. Polymethylmethacrylate composites: disturbed bone formation at the surface of bioactive glass and hydroxyapatite. *Biomaterials.* 1996;17(18):1755-1760.
37. Shinzato S, Nakamura T, Ando K, Kokubo T, Kitamura Y. Mechanical properties and osteoconductivity of new bioactive composites consisting of partially crystallized glass beads and poly(methyl methacrylate). *Journal of Biomedical Materials Research.* 2002;60(4):556-563.
38. Gristina AG. Biomaterial-Centered Infection: Microbial Adhesion Versus Tissue Integration. *Science.* 1987;237(4822):1588-1595.
39. Dunne N, Hill J, McAfee P, et al. In vitro study of the efficacy of acrylic bone cement loaded with supplementary amounts of gentamicin: effect on mechanical properties, antibiotic release, and biofilm formation. *Acta Orthop.* 2007;78(6):774-785.
40. ASTM International. ASTM F451-16 Standard Specification for Acrylic Bone Cement. West Conshohocken, PA: ASTM International, 2016. doi: https://doi-org.www2.lib.ku.edu/10.1520/F0451-16.
41. Neut D, van de Belt H, van Horn JR, van der Mei HC, Busscher HJ. Residual gentamicin-release from antibiotic-loaded polymethylmethacrylate beads after 5 years of implantation. *Biomaterials.* 2003;24(10):1829-1831.
42. Kokubo T, Takadama H. How useful is SBF in predicting in vivo bone bioactivity? *Biomaterials.* 2006;27(15):2907-2915.
43. Fujibayashi S, Neo M, Kim H-M, Kokubo T, Nakamura T. A comparative study between in vivo bone ingrowth and in vitro apatite formation on Na2O–CaO–SiO2 glasses. *Biomaterials.* 2003;24(8):1349-1356.
44. Liu X, Xie Z, Zhang C, et al. Bioactive borate glass scaffolds: in vitro and in vivo evaluation for use as a drug delivery system in the treatment of bone infection. *Journal of Materials Science: Materials in Medicine.* 2010;21(2):575-582.
45. Zhang Y, Cui X, Zhao S, et al. Evaluation of injectable strontium-containing borate bioactive glass cement with enhanced osteogenic capacity in a critical-sized rabbit femoral condyle defect model. *ACS Appl Mater Interfaces.* 2015;7(4):2393-2403.
46. Deliormanli AM. Synthesis and characterization of cerium- and gallium-containing borate bioactive glass scaffolds for bone tissue engineering. *J Mater Sci Mater Med.* 2015;26(2):67.
47. Ding H, Zhao C-J, Cui X, et al. A Novel Injectable Borate Bioactive Glass Cement as an Antibiotic Delivery Vehicle for Treating Osteomyelitis. *PLoS ONE.* 2014;9(1):e85472.
48. Zhang X, Jia W, Gu Y, et al. Teicoplanin-loaded borate bioactive glass implants for treating chronic bone infection in a rabbit tibia osteomyelitis model. *Biomaterials.* 2010;31(22):5865-5874.
49. Wu C, Miron R, Sculean A, et al. Proliferation, differentiation and gene expression of osteoblasts in boron-containing associated with dexamethasone deliver from mesoporous bioactive glass scaffolds. *Biomaterials.* 2011;32(29):7068-7078.
50. Jones JR. Review of bioactive glass: from Hench to hybrids. *Acta Biomater.* 2013;9(1):4457-4486.
51. Lepry WC, Nazhat SN. Highly Bioactive Sol-Gel-Derived Borate Glasses. *Chemistry of Materials.* 2015;27(13):4821-4831.
52. Brink M. The influence of alkali and alkaline earths on the working range for bioactive glasses. *Journal of Biomedical Materials Research.* 1997;36(1):109-117.

53. Fu Q, Rahaman MN, Bal BS, Brown RF, Day DE. Mechanical and in vitro performance of 13-93 bioactive glass scaffolds prepared by a polymer foam replication technique. *Acta Biomater.* 2008;4(6):1854-1864.
54. Liu X, Rahaman MN, Fu Q. Oriented bioactive glass (13-93) scaffolds with controllable pore size by unidirectional freezing of camphene-based suspensions: Microstructure and mechanical response. *Acta Biomater.* 2011;7(1):406-416.
55. Munukka E, Lepparanta O, Korkeamaki M, et al. Bactericidal effects of bioactive glasses on clinically important aerobic bacteria. *J Mater Sci Mater Med.* 2008;19(1):27-32.
56. Oliveira R, Melo L, Oliveira A, Salgueiro R. Polysaccharide production and biofilm formation by Pseudomonas fluorescen: effects of pH and surface material. *Colloids and Surfaces B: Biointerfaces.* 1994;2(1):41-46.
57. Zhang D, Lepparanta O, Munukka E, et al. Antibacterial effects and dissolution behavior of six bioactive glasses. *J Biomed Mater Res A.* 2010;93(2):475-483.
58. Fu Q, Rahaman MN, Fu H, Liu X. Silicate, borosilicate, and borate bioactive glass scaffolds with controllable degradation rate for bone tissue engineering applications. I. Preparation and in vitro degradation. *J Biomed Mater Res A.* 2010;95(1):164-171.
59. Rahaman MN, Day DE, Bal BS, et al. Bioactive glass in tissue engineering. *Acta Biomater.* 2011;7(6):2355-2373.
60. Stone-Weiss N, Pierce EM, Youngman RE, et al. Understanding the structural drivers governing glass-water interactions in borosilicate based model bioactive glasses. *Acta Biomater.* 2017.
61. Huang W, Day DE, Kittiratanapiboon K, Rahaman MN. Kinetics and mechanisms of the conversion of silicate (45S5), borate, and borosilicate glasses to hydroxyapatite in dilute phosphate solutions. *Journal of Materials Science: Materials in Medicine.* 2006;17(7):583-596.
62. Nielsen FH, Stoecker BJ. Boron and fish oil have different beneficial effects on strength and trabecular microarchitecture of bone. *J Trace Elem Med Biol.* 2009;23(3):195-203.
63. Kamitsos EI. Modifying Role of Alkali-Metal Cations in Borate Glass Networks. *Journal of Physical Chemistry.* 1989;93(4):1604-1611.
64. Yao A, Wang D, Huang W, Fu Q, Rahaman MN, Day DE. In Vitro Bioactive Characteristics of Borate-Based Glasses with Controllable Degradation Behavior. *Journal of the American Ceramic Society.* 2007;90(1):303-306.
65. Diba M, Tapia F, Boccaccini AR, Strobel LA. Magnesium-Containing Bioactive Glasses for Biomedical Applications. *International Journal of Applied Glass Science.* 2012;3(3):221-253.
66. Soulie J, Nedelec JM, Jallot E. Influence of Mg doping on the early steps of physico-chemical reactivity of sol-gel derived bioactive glasses in biological medium. *Phys Chem Chem Phys.* 2009;11(44):10473-10483.
67. Percival M. Bone Health & Osteoporosis. *Applied Nutritional Science Reports.* 1999;5(4):1-6.
68. Zreiqat H, Howlett CR, Zannettino A, et al. Mechanisms of magnesium-stimulated adhesion of osteoblastic cells to commonly used orthopaedic implants. *Journal of Biomedical Materials Research.* 2002;62(2):175-184.
69. Liu X, Rahaman MN, Day DE. Conversion of melt-derived microfibrous borate (13-93B3) and silicate (45S5) bioactive glass in a simulated body fluid. *J Mater Sci Mater Med.* 2013;24(3):583-595.

70. Bertoni E, Bigi A, Cojazzi G, Gandolfi M, Panzavolta S, Roveri N. Nanocrystals of magnesium and fluoride substituted hydroxyapatite. *Journal of Inorganic Biochemistry.* 1998;72(1):29-35.
71. Balasubramanian P, Grünewald A, Detsch R, et al. Ion Release, Hydroxyapatite Conversion, and Cytotoxicity of Boron-Containing Bioactive Glass Scaffolds. *International Journal of Applied Glass Science.* 2016;7(2):206-215.
72. van de Belt H, Neut D, Schenk W, van Horn JR, van der Mei HC, Busscher HJ. Infection of orthopedic implants and the use of antibiotic-loaded bone cements: A review. *Acta Orthopaedica Scandinavica.* 2001;72(6):557-571.
73. Rahaman MN, Bal BS, Huang W. Review: emerging developments in the use of bioactive glasses for treating infected prosthetic joints. *Mater Sci Eng C Mater Biol Appl.* 2014;41:224-231.
74. Hanssen AD. Local Antibiotic Delivery Vehicles in the Treatment of Musculoskeletal Infection. *Clinical Orthopaedics & Related Research.* 2005;437:91-96.
75. Mader JT, Calhoun J, Cobos J. In Vitro Evaluation of Antibiotic Diffusion from Antibiotic-Impregnated Biodegradable Beads and Polymethylmethacrylate Beads. *Antimicrobial Agents and Chemotherapy.* 1997;41(2):415-418.
76. Neut D, van de Belt H, Stokroos I, van Horn JR, van der Mei HC, Busscher HJ. Biomaterial-associated infection of gentamicin-loaded PMMA beads in orthopaedic revision surgery. *Journal of Antimicrobial Chemotherapy.* 2001;47(6):885-891.
77. Shinzato S, Nakamura T, Kokubo T, Kitamura Y. Bioactive bone cement: Effect of filler size on mechanical properties and osteoconductivity. *Journal of Biomedical Materials Research.* 2001;56(3):452-458.
78. Shinzato S, Nakamura T, Kokubo T, Kitamura Y. PMMA-based bioactive cement: Effect of glass bead filler content and histological change with time. *Journal of Biomedical Materials Research.* 2002;59(2):225-232.
79. Shinzato S, Nakamura T, Kokubo T, Kitamura Y. A new bioactive bone cement: Effect of glass bead filler content on mechanical and biological properties. *Journal of Biomedical Materials Research.* 2001;54(4):491-500.
80. Arcos D, Ragel CV, Vallet-Regi M. Bioactivity in glass/PMMA composites used as drug delivery system. *Biomaterials.* 2001;22:701-708.
81. Fernández M, Méndez JA, Vázquez B, et al. Acrylic-phosphate glasses composites as self-curing controlled delivery systems of antibiotics. *Journal of Materials Science: Materials in Medicine.* 2002;13(12):1251-1257.
82. K. Kuechle D, C. Landon G, M. Musher D, Noble P. *Elution of Vancomycin, Daptomycin, and Amikacin From Acrylic Bone Cement.* Vol &NA;1991.
83. Huiskes RIK, Weinans H, Van Rietbergen B. *The Relationship Between Stress Shielding and Bone Resorption Around Total Hip Stems and the Effects of Flexible Materials.* Vol 2741992.
84. Mozafari M, Rabiee M, Azami M, Maleknia S. Biomimetic formation of apatite on the surface of porous gelatin/bioactive glass nanocomposite scaffolds. *Applied Surface Science.* 2010;257(5):1740-1749.
85. Fujita H, Ido K, Matsuda Y, et al. Evaluation of bioactive bone cement in canine total hip arthroplasty. *Journal of Biomedical Materials Research.* 2000;49(2):273-288.

86. Ayre WN, Denyer SP, Evans SL. Ageing and moisture uptake in polymethyl methacrylate (PMMA) bone cements. *Journal of the Mechanical Behavior of Biomedical Materials.* 2014;32:76-88.
87. Liu X, Rahaman MN, Day DE, Bose S. In Vitro Degradation and Conversion of Melt-Derived Microfibrous Borate (13-93B3) Bioactive Glass Doped with Metal Ions. *Journal of the American Ceramic Society.* 2014;97(11):3501-3509.
88. Cui X, Gu Y, Li L, et al. In vitro bioactivity, cytocompatibility, and antibiotic release profile of gentamicin sulfate-loaded borate bioactive glass/chitosan composites. *J Mater Sci Mater Med.* 2013;24(10):2391-2403.
89. Lopes PP, Ferreira BJML, Gomes PS, Correia RN, Fernandes MH, Fernandes MHV. Silicate and borate glasses as composite fillers: a bioactivity and biocompatibility study. *Journal of Materials Science: Materials in Medicine.* 2011;22(6):1501-1510.
90. Bi L, Rahaman MN, Day DE, et al. Effect of bioactive borate glass microstructure on bone regeneration, angiogenesis, and hydroxyapatite conversion in a rat calvarial defect model. *Acta Biomater.* 2013;9(8):8015-8026.
91. Lopes PP, Garcia MP, Fernandes MH, Fernandes MH. Acrylic formulations containing bioactive and biodegradable fillers to be used as bone cements: properties and biocompatibility assessment. *Mater Sci Eng C Mater Biol Appl.* 2013;33(3):1289-1299.
92. Hamizah AS, Mariatti M, Othman R, Kawashita M, Noor Hayati AR. Mechanical and thermal properties of polymethylmethacrylate bone cement composites incorporated with hydroxyapatite and glass-ceramic fillers. *Journal of Applied Polymer Science.* 2012;125(S1):E661-E669.
93. ISO 5833:2002 - Implants for Surgery - Acrylic Resin Cements. International Organization for Standardization, Geneva, Switzerland.
94. Fu S-Y, Feng X-Q, Lauke B, Mai Y-W. Effects of particle size, particle/matrix interface adhesion and particle loading on mechanical properties of particulate–polymer composites. *Composites Part B: Engineering.* 2008;39(6):933-961.
95. Damadzadeh B, Jabari H, Skrifvars M, Airola K, Moritz N, Vallittu PK. Effect of ceramic filler content on the mechanical and thermal behaviour of poly-L-lactic acid and poly-L-lactic-co-glycolic acid composites for medical applications. *J Mater Sci Mater Med.* 2010;21(9):2523-2531.
96. Boesel LF, Reis RL. A review on the polymer properties of Hydrophilic, partially Degradable and Bioactive acrylic Cements (HDBC). *Progress in Polymer Science.* 2008;33(2):180-190.
97. Abdelghany AM. Novel method for early investigation of bioactivity in different borate bio-glasses. *Spectrochim Acta A Mol Biomol Spectrosc.* 2013;100:120-126.
98. JL G. *Dissolution of Borate Glasses and Precipitation of Phosphate Compounds* [Thesis]. Scholars' Mine: Materials Science and Engineering, Missouri University of Science and Technology; Spring 2015.
99. Liu X, Huang W, Fu H, et al. Bioactive borosilicate glass scaffolds: in vitro degradation and bioactivity behaviors. *J Mater Sci Mater Med.* 2009;20(6):1237-1243.
100. Weinstein RA, Darouiche RO. Device-Associated Infections: A Macroproblem that Starts with Microadherence. *Clinical Infectious Diseases.* 2001;33(9):1567-1572.
101. Thewes N, Thewes A, Loskill P, et al. Stochastic binding of Staphylococcus aureus to hydrophobic surfaces. *Soft Matter.* 2015;11(46):8913-8919.

102. Kamimura M, Tamura J, Shinzato S, et al. Interfacial tensile strength between polymethylmethacrylate-based bioactive bone cements and bone. *Journal of Biomedical Materials Research.* 2002;61(4):564-571.
103. Kappler A, Fischer D, Oberbeckmann S, et al. Analysis of environmental microplastics by vibrational microspectroscopy: FTIR, Raman or both? *Anal Bioanal Chem.* 2016;408(29):8377-8391.
104. Kimura-Suda H, Ito T. Bone quality characteristics obtained by Fourier transform infrared and Raman spectroscopic imaging. *Journal of Oral Biosciences.* 2017;59(3):142-145.
105. Willis HA, Zichy VJI, Hendra PJ. The laser-Raman and infra-red spectra of poly(methyl methacrylate). *Polymer.* 1969;10:737-746.
106. Kamitsos EI, Karakassides MA, Chryssikos GD. Vibrational Spectra of Magnesium-Sodium-Borate Glasses. 2. Raman and Mid-Infrared Investigation of the Network Structure. *J Phys Chem,.* 1987;91(5):1073-1079.
107. Morgan H, Wilson RM, Elliott JC, Dowker SEP, Anderson P. Preparation and characterisation of monoclinic hydroxyapatite and its precipitated carbonate apatite intermediate. *Biomaterials.* 2000;21(6):617-627.
108. Rehman I, Bonfield W. Characterization of hydroxyapatite and carbonated apatite by photo acoustic FTIR spectroscopy. *Journal of Materials Science: Materials in Medicine.* 1997;8(1):1-4.
109. Shen Y, Li C, Zhu X, Xie A, Qiu L, Zhu J. Study on the preparation and formation mechanism of barium sulphate nanoparticles modified by different organic acids. *Journal of Chemical Sciences.* 2007;119(4):319-324.
110. Mori S. Compositional analysis and infrared spectra of styrene–methyl methacrylate random copolymers. *Journal of Applied Polymer Science.* 1989;38(3):547-555.
111. MRHM H, S K, S M. FT-IR and FT-Raman Spectra and Normal Coordinate Analysis of Poly methyl methacrylate. *Der Pharma Chemica.* 2010;2(4):316-323.
112. Farzadi A, Bakhshi F, Solati-Hashjin M, Asadi-Eydivand M, Osman NAa. Magnesium incorporated hydroxyapatite: Synthesis and structural properties characterization. *Ceramics International.* 2014;40(4):6021-6029.
113. Penel G, Leroy G, Rey C, Bres E. MicroRaman Spectral Study of the PO4 and CO3 Vibrational Modes in Synthetic and Biological Apatites. *Calcified Tissue International.* 1998;63(6):475-481.
114. Xingsheng X, Hai M, Qijing Z, Yunsheng Z. Properties of Raman spectra and laser-induced birefringence in polymethyl methacrylate optical fibres. *Journal of optics A Pure and Applied Optics.* 2002;4:237-242.
115. Pei-Lun Lee VL, Eugene Huang VL, Shu-Cheng Yu VL. High-pressure Raman and X-ray studies of barite, BaSO 4. *High Pressure Research.* 2003;23(4):439-450.
116. Sears WM, Hunt JL, Stevens JR. Raman scattering from polymerizing styrene. I. Vibrational mode analysis. *The Journal of Chemical Physics.* 1981;75(4):1589-1598.
117. Matsushita A, Ren Y, Matsukawa K, et al. Two-dimensional Fourier-transform Raman and near-infrared correlation spectroscopy studies of poly(methyl methacrylate) blends. *Vibrational Spectroscopy.* 2000;24(2):171-180.
118. Han GS, Lee S, Kim DW, et al. A Simple Method To Control Morphology of Hydroxyapatite Nano- and Microcrystals by Altering Phase Transition Route. *Crystal Growth & Design.* 2013;13(8):3414-3418.

119. Kobayashi T, Ono S, Hirakura S, Oaki Y, Imai H. Morphological variation of hydroxyapatite grown in aqueous solution based on simulated body fluid. *CrystEngComm.* 2012;14(3):1143-1149.
120. Fu Q, Rahaman MN, Bal BS, Bonewald LF, Kuroki K, Brown RF. Silicate, borosilicate, and borate bioactive glass scaffolds with controllable degradation rate for bone tissue engineering applications. II. In vitro and in vivo biological evaluation. *J Biomed Mater Res A.* 2010;95(1):172-179.
121. Bertinetti L, Drouet C, Combes C, et al. Surface Characteristics of Nanocrystalline Apatites: Effect of Mg Surface Enrichment on Morphology, Surface Hydration Species, and Cationic Environments. *Langmuir.* 2009;25(10):5647-5654.
122. Yang X, Xie B, Wang L, Qin Y, Henneman ZJ, Nancollas GH. Influence of magnesium ions and amino acids on the nucleation and growth of hydroxyapatite. *CrystEngComm.* 2011;13(4):1153-1158.
123. Pleshko N, Boskey A, Mendelsohn R. Novel infrared spectroscopic method for the determination of crystallinity of hydroxyapatite minerals. *Biophysical Journal.* 1991;60(4):786-793.
124. Termine J, Posner A. Infra-red Determination of the Precentage of Crystallinity in Apatitic Calcium Phosphates. *Nature.* 1966;211:268-270.
125. Kaniappan K, Latha S. Certain Investigations on the Formulation and Characterization of Polystyrene/Poly (methyl methacrylate) Blends. *International Journal of ChemTech Research.* 2011;3(2):708-711.
126. Saber-Samandari S, Alamara K, Saber-Samandari S. Calcium phosphate coatings: Morphology, micro-structure and mechanical properties. *Ceramics International.* 2014;40(1):563-572.
127. de Aza PN, Guitián F, Santos C, de Aza S, Cuscó R, Artús L. Vibrational Properties of Calcium Phosphate Compounds. 2. Comparison between Hydroxyapatite and β-Tricalcium Phosphate. *Chemistry of Materials.* 1997;9(4):916-922.
128. Yuan X, Zhu B, Tong G, Su Y, Zhu X. Wet-chemical synthesis of Mg-doped hydroxyapatite nanoparticles by step reaction and ion exchange processes. *Journal of Materials Chemistry B.* 2013;1(47):6551.
129. Chaudhry AA, Goodall J, Vickers M, et al. Synthesis and characterisation of magnesium substituted calcium phosphate bioceramic nanoparticles made via continuous hydrothermal flow synthesis. *Journal of Materials Chemistry.* 2008;18(48):5900-5908.
130. Sprio S, Pezzotti G, Celotti G, Landi E, Tampieri A. Raman and cathodoluminescence spectroscopies of magnesium-substituted hydroxyapatite powders. *Journal of Materials Research.* 2005;20(4):1009-1016.
131. Kaur G, Pandey OP, Singh K, Homa D, Scott B, Pickrell G. A review of bioactive glasses: Their structure, properties, fabrication and apatite formation. *Journal of Biomedical Materials Research Part A.* 2014;102(1):254-274.

Appendix

Appendix 1-1: An extended version of Figure 2-1 showing the respective control data for compressive strength that the composites were compared against for statistical analysis. The lines intersecting the graphs correspond to 70 MPa, the minimum standard from ASTM F451 and ISO 5833. A diamond (♦) represents a group that soaked for 20 days. A triangle (▲) represents a group of n=4. An asterisk (*) over composite data represents a significant difference ($p<0.05$) from its respective control.

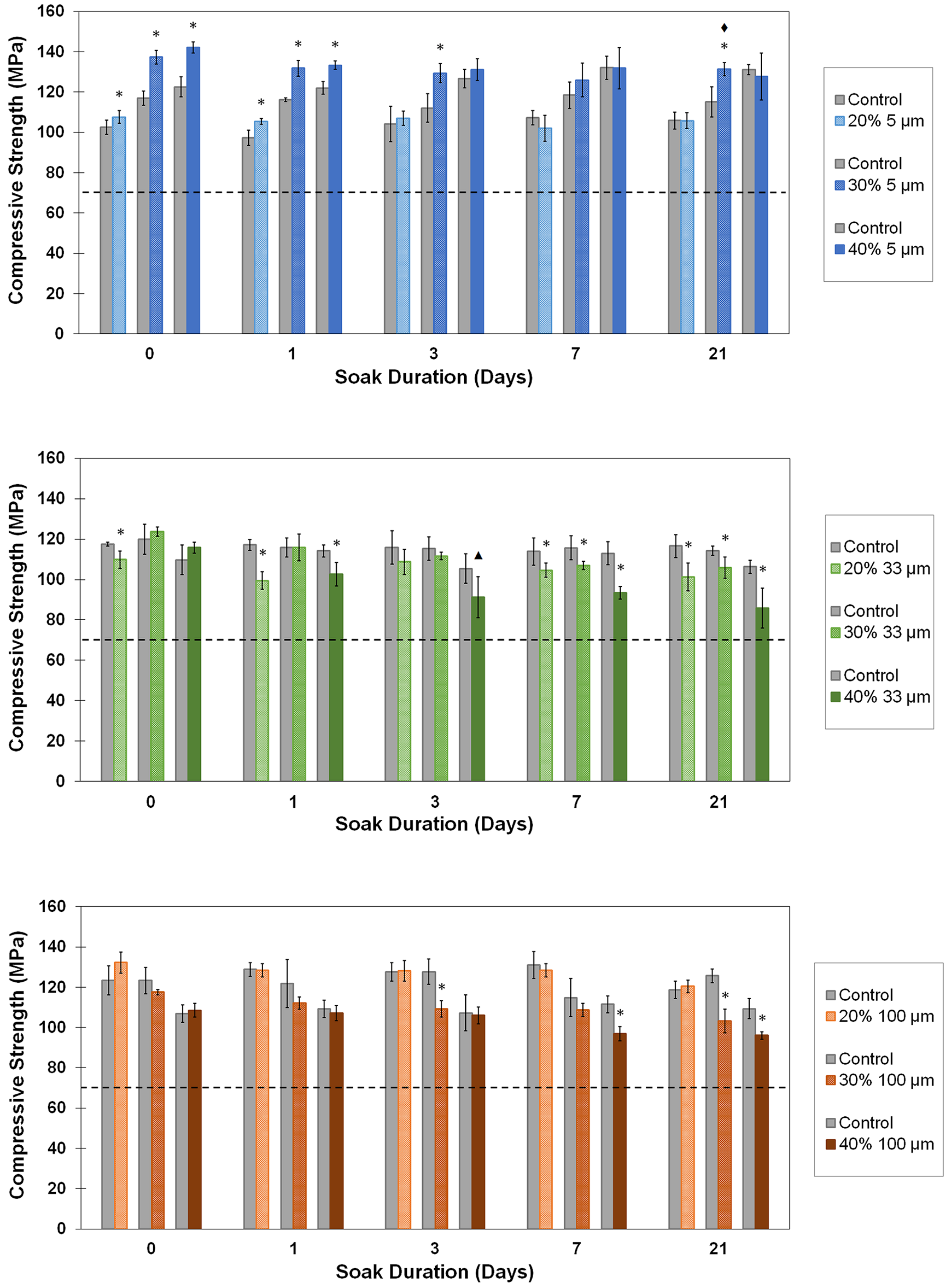

Appendix 1-2: An extended version of Figure 2-2 showing the respective control data for Young’s modulus that the composites were compared against for statistical analysis. A diamond (♦) represents a group that soaked for 20 days. A triangle (▲) represents a group of n=4. An asterisk (*) over composite data represents a significant difference ($p<0.05$) from its respective control.

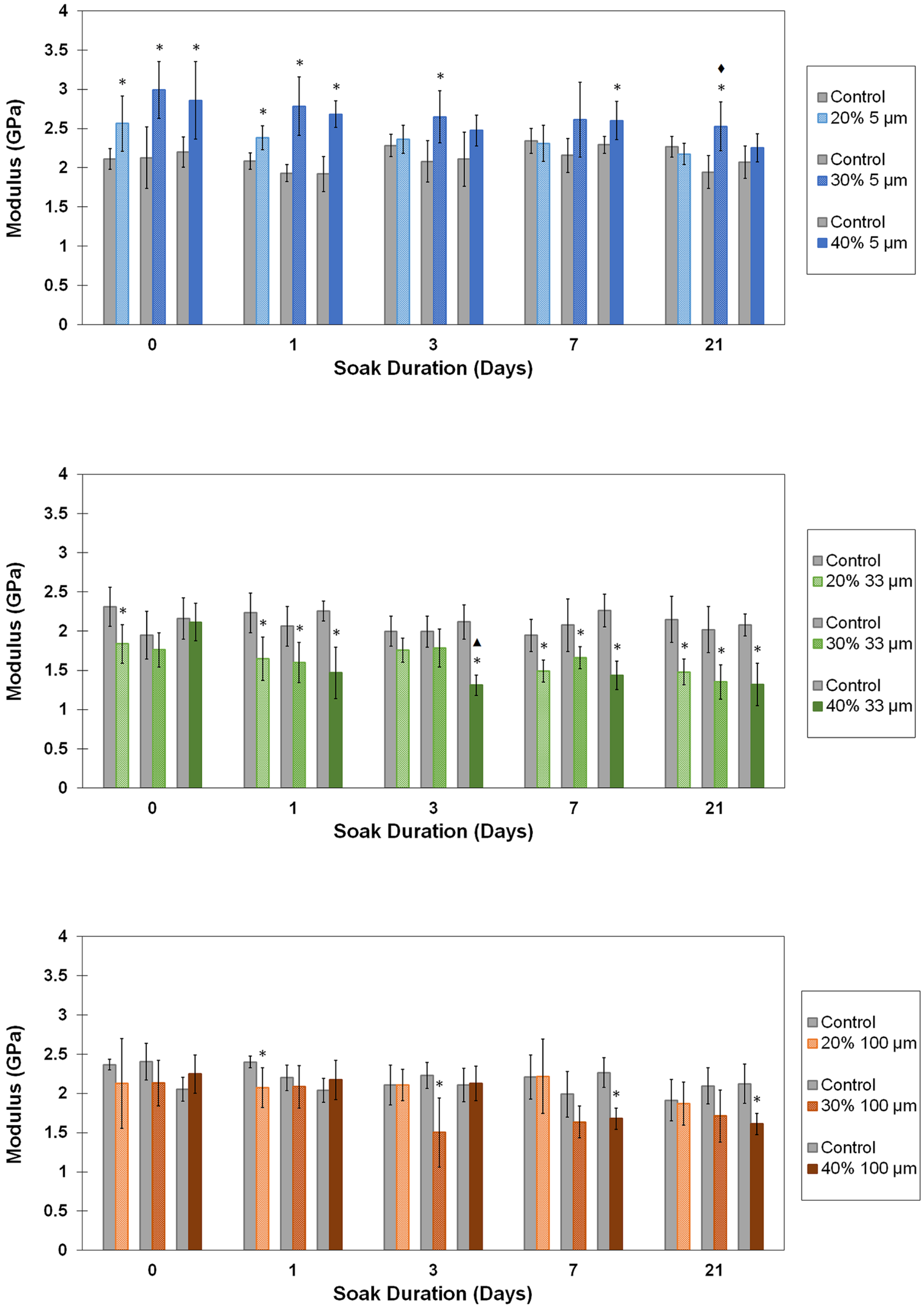

Appendix 1-3: An extended version of Figure 2-3 showing the respective control data for weight loss that the composites were compared against for statistical analysis. An asterisk (*) over composite data represents a significant difference (p<0.05) from its respective control.

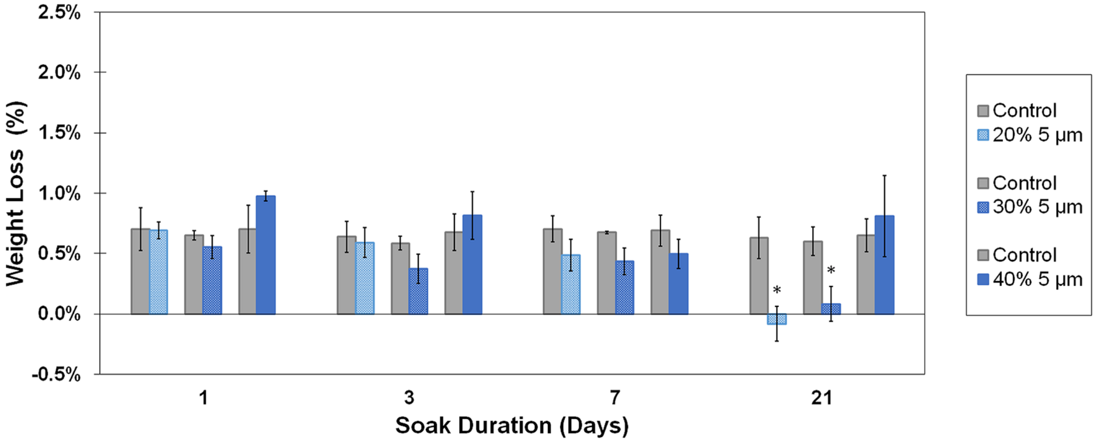

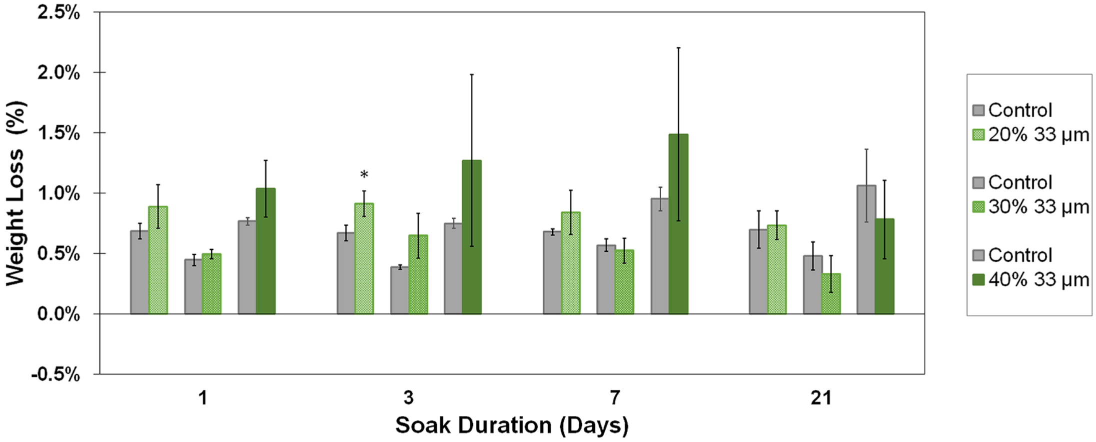

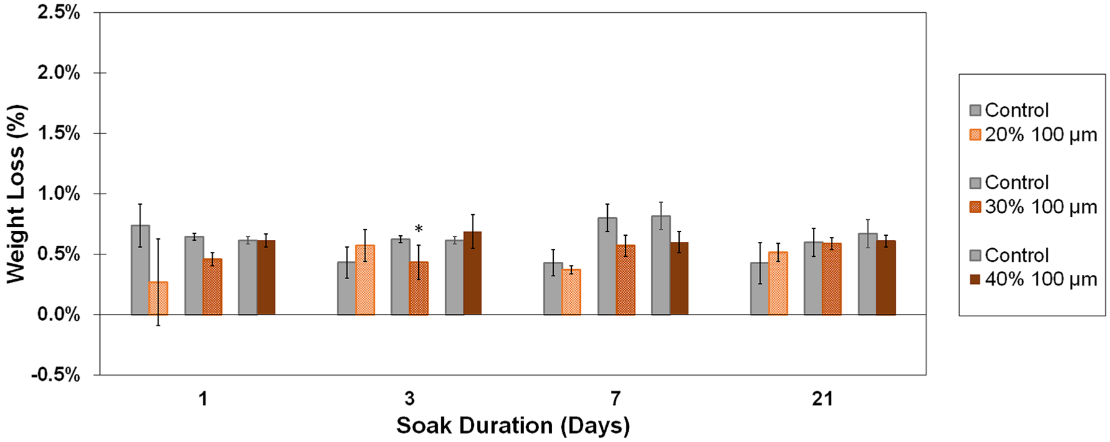

Appendix 1-4: An extended version of Figure 2-4 showing the respective control data for water uptake that the composites were compared against for statistical analysis. An asterisk (*) represents a significant difference ($p<0.05$) from its respective control.